AN EXPERIMENTAL INVESTIGATION

OF TURBOCHARGER STALL

by

VINCENT RALPH CAPECE

B.S., Tennessee Technological University
(1980)

SUBMITTED TO THE DEPARTMENT OF
MECHANICAL ENGINEERING IN PARTIAL
FULFILLMENT OF THE
REQUIREMENTS FOR THE
DEGREE OF

MASTER OF SCIENCE IN
MECHANICAL ENGINEERING

at the

MASSACHUSETTS INSTITUTE OF TECHNOLOGY

June 1982

Signature of Author _____
Department of Mechanical Engineering
May 18, 1982

Certified by _____
Edward M. Greitzer
Thesis Supervisor

Accepted by _____
Warren M. Rohsenow
Chairman, Departmental Graduate Committee

AN EXPERIMENTAL INVESTIGATION

OF TURBOCHARGER STALL

by

VINCENT RALPH CAPECE

Submitted to the Department of Mechanical Engineering
on May 18, 1982 in partial fulfillment of the
requirements for the Degree of Master of Science in
Mechanical Engineering

ABSTRACT

The present investigation deals with the first phases of an ongoing project. These are the design and construction of a turbocharger test facility, the overall steady-state performance map, and the initial results from the high response instrumentation concerning centrifugal compressor stall. The test facility was designed so the compressor would operate at a pressure ratio of 2.0 and a mass flow of 50 LBm/min. To accomplish this goal an air ejection system was designed using the compressor exhaust and the Gas Turbine Laboratory high pressure air supply. In addition, an exhauster was used to reduce the turbine exit static pressure below atmospheric in order to increase the turbine work. The overall performance of the compressor was measured at four different rotational speeds, and it was found that the surge points depend upon the amount of throttling of the valve at compressor exit. Dynamic response pressure measurements taken in the inducer region of the impeller indicated that rotating stall may be present in the impeller preceding system surge. The surge frequency was found to be 28 Hz.

Thesis Supervisor: Dr. Edward M. Greitzer

Title: Professor of Aeronautics and Astronautics

ACKNOWLEDGEMENTS

This work was supported by Cummins Engine Company, Dr. H. G. Weber, technical monitor.

The author wishes to express his gratitude to many members of the Gas Turbine Laboratory staff for their assistance in the construction and operation of this experiment. In particular, I wish to acknowledge Professor E. M. Greitzer for his guidance and Professor E. E. Covert for his help in the selection of the dynamic response probes and in the vibration analysis of the compressor frame. Special thanks is extended to J. Marksteiner, G. Paluccio, and V. Dubrowski for their knowledge and craftsmanship in the mechanical aspects. I also wish to thank T. Eastland for his help in designing the computer hardware and software, and G. Power for his encouragement and technical assistance.

Most of all, the author thanks his wife, Jeanine, for her encouragement and understanding over the past four years. Also, her typing of this manuscript is greatly appreciated. To her this thesis is dedicated.

TABLE OF CONTENTS

TABLE OF CONTENTS (CONTINUED)

LIST OF TABLES

LIST OF FIGURES

Figure

NOMENCLATURE

A	mixing tube cross-sectional area
Cp	static pressure rise coefficient
C_x	axial velocity
D	mixing tube diameter
D_E	nozzle exit diameter
^oC	degrees Celsius
^oF	degrees Fahrenheit
^oR	degrees Rankine
δ^*	displacement thickness
D_{inlet}	inlet diameter
D_{throat}	throat diameter
F_e	function of Cp_{exit}
$F(\Theta)$	function defined by equation A.6
ft	feet
γ	specific heat ratio
g_c	gravitational constant
Hz	Hertz
G_i	function of Cp_{inlet}
in, "	inch
K_L	valve loss coefficient
λ	function defined by equation A.9
LBm	pounds mass
L_c	length of convergent portion of nozzle
M	Mach number
m	D_{inlet}/D_{throat}

$\dot{m}$	mass flow
min	minute
N	Mach number function
ω	constant
P	pressure
ψ	Prandtl-Meyer expansion angle
psi	pounds per square inch
psia	absolute pressure
psig	gauge pressure
R	gas constant
Re	Reynolds number
ρ	density
RPM	revolutions per minute
sec	second
τ	defined by equation A.2
Θ	defined by equation A.5
T	temperature
U	inducer tip speed
V	velocity
X	X_m/L_c; see Figure A-2
x	horizontal axis
x_m	location of inflection point; see Figure A-2
x_o	defined by equation A.8
y	vertical axis

Subscripts

1,2	station locations
ATM	atmospheric
CL	center line
i	primary stream
MAX	maximum
o	secondary stream
T	total or stagnation properties

CHAPTER 1

INTRODUCTION AND LITERATURE REVIEW

1.1 INTRODUCTION

Under normal operating conditions a compressor exhibits a steady and axisymmetric flow, aside from the blade to blade pressure variations and the small scale unsteadiness associated with the moving pressure and velocity fields. However, if the performance map of a compressor is plotted in the form of pressure ratio versus corrected mass flow for different rotational speeds, a limiting line is found which separates stable operation from unstable operation. This line is often defined as the "stall" line, and steady flow generally does not occur to the left of this line (see Figure 1).

When the stall line is encountered the resulting phenomena can take one of two forms: rotating stall or surge. In surge the compressor experiences large amplitude fluctuations in the total annulus average flow, while in rotating stall one to several cells of severely stalled flow are found to rotate around the circumference, although the annulus averaged flow is independent of time once the stall cells become fully developed. In some cases a combination of both phenomena may appear.

Significant progress has been made in the understanding of surge and rotating stall in axial flow compressors. In multistage axial flow compressors the sequence of events seems to be local rotating stall followed by system surge. However, there is a lack of fundamental

understanding of the occurrence of these phenomena in centrifugal compressors. Reviewing the literature one finds disagreement between the experts on what "triggers" surge in centrifugal compressors.

For these reasons a basic research program was undertaken to obtain systematic experimental data from which the mechanisms of these phenomena occurring in centrifugal compressors (turbochargers, in this case), may be explained. As an example, specific questions that can be addressed are:

- Is it the onset of rotating stall that causes surge?
- What is the influence of overall system parameters on the "surge point"?
- Is surge breakdown axisymmetric?
- Can one portion of the impeller be associated with stall?
- How does the diffuser (vaned or vaneless) influence surge?

In order to investigate these topics, a turbocharger compressor was instrumented with high response pressure probes. The compressor was also equipped with steady-state instrumentation so that the characteristic of both the impeller and vaneless diffuser could be found.

This project is an ongoing one and the present report deals only with the first phases of the work. These are the design and construction of a suitable turbocharger test facility, the steady-state performance maps, and the initial results from the high response instrumentation concerning centrifugal compressor stall.

1.2 LITERATURE REVIEW

One of the first definitive studies which separated surge and rotating stall into two distinct phenomena was conducted by Emmons, Pearson, and Grant [9]. The centrifugal compressor used in this study contained an axial flow inducer blade row, a straight radial bladed impeller (no backsweep), followed by a vaneless diffuser and collector case. The inducer and impeller were separated by a small axial gap.

This compressor produced characteristics of three distinct types. The first type was at low rotational speeds. The curve of pressure ratio versus mass flow was negatively sloped from maximum flow to near zero flow, with a steep drop in pressure and deeply pulsating flow (deep surge) occurring at very low flows.

The second type was exhibited at slightly higher rotational speeds, where a double peaked curve was encountered. As the flow was decreased from maximum flow to the first peak, mild pulsating flow (mild surge) was present. With further reduction in flow, the mild surge ceased and rotating stall was present in the axial bladed inducer. At still lower flows the rotating stall disappeared, the second peak was encountered and deep surge was found. Finally, at high rotational speeds the pressure ratio rose rapidly with slight reduction in flow, to a peak where deep surge was encountered.

It was discovered that the zones of mild and deep surge merged at high rotational speeds, thus precluding the appearance of mild surge and inducer rotating stall preceding the deep surge region. However, no information was given about the vaneless diffuser's influence on system stability.

Amann and Nordenson [3] also found that the centrifugal compressor they used exhibited the phenomena of mild and deep surge separated by a

zone of inducer rotating stall at low speed (an impeller tip speed of 1019 ft/sec). As the impeller tip speed increased, the region of rotating stall disappeared and mild surge preceded the zone of deep surge. Upon reducing the flow at high impeller tip speeds, deep surge was encountered without any preceding zone of mild surge.

A vaned diffuser was used in this investigation and it was found that by its redesign, the surge line could be moved further to the left without any degradation in compressor efficiency during normal operation. However, although the surge margin was improved (at high rotational speeds and low flows), the entire speed line was also shifted to the left by the same amount.

The diffuser's influence on system stability was also emphasized in the study by Toyama, Runstadler and Dean [35]. The measurements were focused upon the impeller exit/diffuser inlet region. In this location, hot-wire, hot-film and dynamic pressure transducers were installed. It was found that when the instantaneous pressure rise coefficient was between .4 and .45 the compressor surged. It previously had been thought that separated flow in the diffuser caused surge, but hot-film measurements showed that the flow separation occurred once flow reversal had already been established. Their measurements gave indications that the surge breakdown was axisymmetric. No measurements were taken to determine the impeller's influence on compressor stability.

Extensive measurements were taken along the shroud of a radial bladed impeller by Bammert and Rautenberg [4] with high response static pressure transducers. They found that at low flows rotating stall occurred after the peak of the pressure rise curve, and upon further reduction of flow, system surge was encountered. The measurements showed that during surge a

period of large scale fluctuations in static pressure preceded a period of rotating stall followed by a period of recovery. After the recovery period the surge cycle was repeated.

Even though the compressor contained a vaneless diffuser, no measurements were taken in this component, their supposition being that the impeller was the element that caused compressor instability at the speed considered.

As can be seen there is conflict of opinion on which component causes a centrifugal compressor to stall. This is particularly evident from the discussions given of Toyama [35]. In these discussions, Balje offers the opinion that surge in centrifugal compressors is a system phenomena and not determined by the machine itself. However, Greitzer and Cumpsty feel that the local events create the conditions that are required for the global type of behavior seen in surge. Bullock is also of the opinion that local events occurring in one component of the compressor cause a system surge. Finally, Jansen [19] states that surge is initiated by compressor component stall, and this component stall is a rotating stall, rather than a flow separation along a blade surface or wall.

So the picture which emerges from the literature is that there is no consensus of opinion on which component causes system instability, or the fluid mechanics which govern the instability. For these reasons a basic investigation studying the phenomena of centrifugal compressor instability is warranted.

CHAPTER 2

TEST FACILITY DESIGN

2.1 INTRODUCTION

As the first phase of this investigation a suitable turbocharger test facility had to be designed. The criterion for the design of the facility was that the system would drive the turbocharger at a reasonable speed over a substantial portion of the stable operating range and be flexible enough to be used on turbocharger projects in the future. A pressure ratio of 2.0 and a mass flow of 50 LBm/min were used as design goals.

After considering several different facilities, an air ejection system was found to best fit the design goals. The ejection system uses the Gas Turbine Laboratory high pressure air supply as the primary stream in the ejector. This air flows through a converging-diverging nozzle into a mixing tube. The exhaust from the turbocharger compressor (the secondary stream) flows into a supply tank and then into the mixing tube. The mixed out flow enters the radial-inflow turbine which then drives the compressor.

The design of this system is described in the following sections. Also discussed in this chapter is the design of the convergent-divergent nozzle, the supply tank, the modelling results, the steam ejector, and the vibration isolation of the compressor.

2.2 AIR EJECTOR

2.2.1 Air Ejector Design

A schematic diagram of a simple air ejection system is shown in Figure 2. The "i" denotes the primary stream (high pressure air) and "o" the secondary stream (compressor exhaust). The high pressure air exhausts from a convergent-divergent nozzle at Station 1 and, through mixing, increases the pressure of the secondary fluid as it passes from a supply tank (at "o") through the mixing tube. At station 2, the quantities are taken to be uniform or "mixed out".

This system is analyzed in a one-dimensional fashion with the following assumptions:

1. Steady, adiabatic flow;
2. Constant (cross-sectional) area mixing;
3. Perfect gas with constant specific heats;
4. Negligible wall friction; and
5. Equal specific heat ratio and gas constant for the two streams.

The usual design procedure for an ejector consists of evaluating the properties at Stations 1 and 2 with the geometry already known. In the present case, the primary and secondary stream properties are known; therefore, geometry and properties at the mixed-out station are to be determined using trial-and-error.

Choosing a mixing tube diameter, the properties at Station 2 and the convergent-divergent nozzle exit area can be determined. A parametric study was thus carried out with mixing tube diameters of 2, 3, 4, and 5 inches, and with primary stream pressures of 75, 100, and 125 psi (these were set by the air supply capabilities). In all cases the primary stream

mass flow was taken to be .5 LBm/sec, with a total temperature of 540°R.

In the calculations, three specific design points were chosen. The points were all at a pressure ratio of 2.0, but at the following compressor mass flow rates: 40, 45, and 50 LBm/min. With these design points, the air ejector system was determined by varying the mixing tube diameter and the primary stream total pressure until the optimum pressure gain through the tube was obtained.

The first step in the design procedure was to choose a primary stream total pressure, and a secondary stream mass flow. The secondary stream Mach number at Station 1 can then be determined using,

$$\frac{\dot{m}_o}{P_{To} A g_c}\sqrt{\frac{RT_{To}g_c}{\gamma}} = M_{o1}\left[1 + \frac{\gamma-1}{2} M_{o1}^2\right]^{-\frac{\gamma+1}{2(\gamma-1)}} \qquad \text{E 2.1}$$

where $\dot{m}_o$ is the secondary stream mass flow (compressor exhaust), T_{To} the secondary stream total temperature, P_{To} the supply tank total pressure, M_{o1} the secondary stream Mach number at Station 1, A the mixing tube cross-sectional area, R the gas constant, γ the specific heat ratio, and g_c the gravitational constant.

The supply tank total pressure, P_{To}, was found by calculating the pressure drop from the compressor exit to the supply tank entrance. This required an estimation of the piping layout between these two components. The preliminary design called for the expansion of the compressor exit flow from the 2.9 inch diameter scroll exit to 4 inch pipe, a gate valve (to control compressor mass flow), and a sudden expansion from the 4 inch pipe to a large reservoir (supply tank) where the velocity would essentially be zero. The pipe length between these two components was assumed to be 15 feet with two 90° elbows.

The secondary stream total temperature was taken as the compressor exit total temperature. This was determined by assuming a compressor total-to-total efficiency of 75% with a pressure ratio of 2.0 and an inlet compressor temperature of 80°F. With the secondary stream Mach number determined, the static pressure at Station 1 could be found.

Since one-dimensional flow is assumed, the static pressures of both streams are equivalent at Station 1, and the primary stream Mach number, M_{i1}, (using the calculated static pressure, P_1) for ideal expansion is thus:

$$M_{i1} = \left[\frac{2}{\gamma - 1} \left(\left(\frac{P_{Ti}}{P_1} \right)^{\frac{\gamma - 1}{\gamma}} - 1 \right) \right]^{1/2} \qquad \text{E 2.2}$$

where P_{Ti} is the primary stream total pressure chosen in step one.

With the properties of both streams defined at Station 1, the next step was to determine the mixed out properties at Station 2. As given by Weatherston [38], the mixed out properties can be determined from the following expression:

$$N_2 = \frac{[(\dot{m}_i + \dot{m}_o)(\dot{m}_i T_{Ti} + \dot{m}_o T_{To})]^{1/2}}{\frac{\dot{m}_i \sqrt{T_{Ti}}}{N_i} + \frac{\dot{m}_o \sqrt{T_{To}}}{N_o}} , \qquad \text{E 2.3a}$$

where the Mach number function, N, is defined as

$$N = \frac{M \left[\left(1 + \frac{\gamma - 1}{2} M^2 \right) \right]^{1/2}}{1 + \gamma M^2} , \qquad \text{E 2.3b}$$

The total pressure at Station 2 is given by,

$$P_{T2} = \frac{(\dot{m}_o + \dot{m}_i)}{A\, g_c} \left(\frac{RT_{T2} g_c}{\gamma}\right)^{1/2} \frac{[1 + \frac{\gamma-1}{2} M_2^2]^{\frac{\gamma+1}{2(\gamma-1)}}}{M_2} \qquad \text{E 2.4}$$

where T_{T2} is the mixed out total temperature determined from an energy balance on the mixing tube. Therefore the ejector performance for the primary stream total pressure, P_{Ti}, and secondary stream mass flow, $\dot{m}_o$, is fully defined.

For the ejector performance given by each of the mixing tube diameters, secondary stream mass flows, and primary stream total pressures, the mixing tube diameter and primary stream total pressure were selected which gave adequate total pressure at Station 2. The primary stream nozzle area was then determined at Station 1 and a convergent-divergent nozzle designed to give the required Mach number. A supply tank and convergent inlet to the mixing tube were also designed to match the chosen system.

2.2.2 Air Ejector Design Results

The results of the air ejector analysis are shown in Figures 3, 4, and 5. In these figures, mixed out total pressure, P_{T2}, is plotted versus mixing tube diameter for each of the secondary flows and primary stream total pressures. The results are shown in dimensional form since they refer to this specific configuration.

From each of these figures it can be seen that the 2 inch diameter mixing tube gave the optimum total pressure gain for the diameters considered. However, at the time, there was a concern about keeping the velocities at the mixing tube exit as low as possible since it was thought that a combustor might be needed in the system to insure the required turbine work. Also, the system had to be kept reasonably short in length

due to space constraints. For these reasons, the mixing tube diameter was chosen to be 3 inches (with the provision to change to the smaller diameter if necessary). As it turned out, a combustor has not been required, so the 3 inch diameter tube could be changed to the smaller diameter tube to take advantage of the higher exit total pressure it offers. To date, however, it has not been necessary to switch to the smaller diameter mixing tube.

With a primary stream pressure of 125 psi, Table 1 summarizes the results of the ejector analysis, with primary stream Mach number and mixed out total pressures given for each secondary stream mass flow. Also shown in this table is the primary stream nozzle exit area at Station 1. The nozzle exit area was calculated by using equation 2.1 for the primary stream with the exit Mach number chosen to be 1.62, since this matched the test facility design goal (50 LBm/min).

Thus with the primary stream total pressure, nozzle exit area, and mixing tube diameter chosen, a convergent-divergent nozzle and a supply tank had to be designed to give the required performance. These are discussed in the next sections.

2.2.3 Convergent-Divergent Nozzle Design

The convergent-divergent nozzle was designed for an exit Mach number of 1.62, and a mass flow of .5 LBm/sec. The analytical technique presented by Foelsch [11] was used to determine the geometry of the divergent portion of the nozzle. It is assumed that the fluid behaves like a perfect gas with constant specific heats.

In this method the necessary information to design the divergent section is the nozzle exit Mach number and area. The x and y coordinates of the wall contour are solved in a step by step fashion. The equations

for these coordinates were derived by integration of the characteristic equations of axially symmetric flow. This analysis contained no boundary layer correction, however, from information found in reference [40], a boundary layer correction was applied to each of the y coordinates of the wall contour.

The convergent portion of the nozzle was designed in accordance with the method presented by Morel [24]. In this method the information necessary to design a nozzle contraction is specified by the values of Cp_{inlet} and Cp_{exit}, the maximum wall pressure coefficients for contraction ratios greater than 4 (the contraction ratio being defined as the nozzle inlet area divided by the throat area). The throat area was calculated as part of the divergent nozzle design and found to be .175 in^2.

The inlet diameter to the convergent portion of the nozzle was chosen to be 2 inches to match the pipe size of the Gas Turbine Laboratory high pressure air supply. To avoid boundary layer separation, the values of Cp_{inlet} and Cp_{exit} were chosen to be .35 and .04, respectively [24].

The nozzle was machined of aluminum and its dimensions are shown in Figure 6. Appendix A includes a detailed description of the procedures used to design the convergent-divergent nozzle.

2.2.4 Supply Tank Design

The supply tank was designed using standard pipe parts. The tank was constructed using a 12 inch length of 6 inch diameter pipe, with standard flanges at each end. A 4 inch pipe was welded to one side of the tank allowing the exhaust from the compressor (secondary stream) to enter.

The end plate for the supply tank through which the high pressure air is supplied to the convergent-divergent nozzle was constructed from a blind

flange (see Appendix B). A round hole was bored in the flange and an O-ring added so that the depth of the nozzle at Station 1 (see Figure 2) could be varied.

The converging entrance to the mixing tube was also designed by Morel's analysis for axisymmetric flow. However, in this case, the contraction was designed so that the inflection point occurred at the inlet, thus providing a smooth contracting section. The coordinates for this design are presented in Appendix B, and the component is shown in Figure 7. Figure 8 shows a diagram of the complete system.

2.2.5 Air Ejector Modelling

Since a one-dimensional analysis (with no mixing tube wall friction) was used in the determination of the ejector geometry, a mixing tube length could not be obtained. Therefore, the length of the mixing tube had to be found experimentally.

Several experimental programs have been carried out on air ejectors [2], [21], [22], [37], and it has been found that the length needed for mixing is between 7 and 10 diameters downstream from Station 1 (see Figure 2). In the mixing tube there is an increase in static pressure (P_2) with length until a maximum is reached, and then a decrease in static pressure with further increase in length. This maximum pressure point determines the mixing tube length.

For simplicity the mixing tube length was determined without using the turbocharger. This required a dimensional analysis of the ejector system with the system parameters being

$$P_{T1i},\ T_{Ti},\ \dot{m}_i,\ \text{and}\ P_{1i}\ \text{or}\ M_{1i}$$

for the primary stream;

$$P_{To},\ T_{To},\ \dot{m}_o,\ \text{and}\ P_{1o}\ \text{or}\ M_{1o}$$

for the secondary stream; and

$$P_{T2},\ T_{T2},\ \dot{m}_2,\ \text{and}\ P_2\ \text{or}\ M_2$$

for the mixed out station. There are eight equations which link the 12 variables listed above. These equations are the continuity equation,

$$\dot{m}_o + \dot{m}_i = \dot{m}_2 \qquad \text{E 2.5}$$

conservation of momentum,

$$A_{1i}[P_{1i} + \gamma M_{1i}^2 P_{1i}] + A_{1o}[P_{1o} + \gamma M_{1o}^2 P_{1o}] = A_2[P_2 + \gamma M_2^2 P_2] \qquad \text{E 2.6}$$

exit static pressure,

$$P_2 = P_{atm} \qquad \text{E 2.7}$$

conservation of energy,

$$\dot{m}_i T_{Ti} + \dot{m}_o T_{To} = \dot{m}_2 T_{T2} \qquad \text{E 2.8}$$

one-dimensional flow,

$$P_{1i} = P_{1o} = P_1 \qquad \text{E 2.9}$$

and the isentropic relationships,

$$\frac{P_{T1i}}{P_1} = \left(1 + \frac{\gamma-1}{2} M_{1i}^2\right)^{\frac{\gamma}{\gamma-1}} \qquad \text{E 2.10}$$

$$\frac{P_{To}}{P_1} = \left(1 + \frac{\gamma-1}{2} M_{1o}^2\right)^{\frac{\gamma}{\gamma-1}} \qquad \text{E 2.11}$$

$$\frac{P_{T2}}{P_2} = \left(1 + \frac{\gamma-1}{2} M_2^2\right)^{\frac{\gamma}{\gamma-1}} \qquad \text{E 2.12}$$

Of these 12 variables, four are controllable (P_{T1i}, P_{To}, T_{To} and T_{Ti}). However, if a throttle valve is placed at the end of the mixing tube, P_2 can also be included as a controllable variable. From these five variables the other seven can be determined.

Thus P_{T2} can be expressed as a function of P_{atm}, M_2, and valve geometry, and equation 2.7 can be replaced by,

$$P_{T2} = P_{atm}\, f(M_2, K_L) \qquad \text{E 2.13}$$

where K_L denotes valve geometry. Therefore the dependent and independent variables can be expressed as

$$T_{T2}, \dot{m}_i, \dot{m}_o, \dot{m}_2, P_1 = \phi(P_{T1i}, P_2, T_{Ti}, P_{To}, T_{To}, P_{atm}, K_L) \qquad \text{E 2.14}$$

This can be nondimensionalized to

$$\frac{P_1}{P_{atm}}, \frac{\dot{m}_2}{\dot{m}_i}, \frac{\dot{m}_o}{\dot{m}_i}, \frac{T_{T2}}{T_{Ti}} = \Phi\left(\frac{P_{Ti}}{P_{atm}}, \frac{P_{To}}{P_{atm}}, \frac{P_2}{P_{atm}}, \frac{T_{Ti}}{T_{To}}, K_L\right) \qquad \text{E 2.15}$$

or

$$\frac{P_1}{P_{atm}}, \frac{\dot{m}_2}{\dot{m}_i}, \frac{\dot{m}_o}{\dot{m}_i}, \frac{T_{T2}}{T_{Ti}} = \psi\left(M_2, \frac{P_{Ti}}{P_{T2}}, \frac{P_{To}}{P_{T2}}, \frac{T_{Ti}}{T_{To}}, K_L\right) \qquad \text{E 2.16}$$

For the dependent variables listed above, the most important is the ratio of the primary to secondary mass flow rates, i.e.,

$$\frac{\dot{m}_o}{\dot{m}_i} = \Psi\left(M_2, \frac{P_{Ti}}{P_{T2}}, \frac{P_{To}}{P_{T2}}, \frac{T_{Ti}}{T_{To}}, K_L\right) \qquad \text{E 2.17}$$

The ejector system was again analyzed so that the design case and modelling case could be compared. An analysis similar to the one presented in Section 2.2.1 was used (the results are shown in Table 2). However, in this case the geometry is already known. Since one-dimensional flow is assumed and the geometry fixed, the exit Mach number, M_{1i}, will be the same as in the design case.

Based on this approach, the mixing tube length can thus be determined using the laboratory air supply only; Chapter 4 shows the results of the experimental determination of tube length.

2.3 STEAM EJECTOR

Although the air ejector increased the total pressure and mass flow rate entering the radial-inflow turbine, it would not run the turbocharger at the design points unless the air was heated to approximately 1100^{o}R. Several means of heating the air to this temperature were examined. However, installing such devices was not desirable because of the additional handling problems and possibilities for instability that may be encountered.

An alternative approach considered was reduction of the turbine exit static pressure. If the back pressure of the turbine was reduced to approximately 13 psia, it was calculated that the system would run at the design points without any combustion device. The Gas Turbine Laboratory has an exhaust system (6 inch Steam Ejector) which was (theoretically) capable of achieving this reduction in turbine back pressure. (Tests had to be run on this system to see if it would achieve the required turbine back pressure; results of these tests are shown in Chapter 4.) By utilizing this Steam Ejector, the test facility is fully specified and is shown in Figure 9.

2.4 VIBRATION ISOLATION

During surge the compressor mass flow undergoes large scale oscillations. These oscillations subject the entire system to alternating vibratory stress levels. Since running the compressor in surge is basic to this investigation, the compressor was isolated from the rest of the test facility. The turbocharger was mounted on a frame which was fixed to a 1/2" x 36" x 36" steel plate. Skid-mate pads were placed on the bottom of the plate to damp out the vibrations. To isolate the turbocharger from the

rest of the system flexible tubing was employed. For the turbine inlet and compressor exit, 3.5 inch diameter flexible tubing was used which had a maximum temperature and pressure rating of 250^{o}F and 22 psig, respectively. The flexible tubing used to connect the turbine exit to the Steam Ejector was 4 inches in diameter and had a pressure rating of 25 inches of mercury vacuum.

CHAPTER 3

FACILITY DESCRIPTION AND INSTRUMENTATION

3.1 TURBOCHARGER

The turbocharger used in this investigation is manufactured by Cummins Engine Company. It consists of a centrifugal compressor and a radial-inflow turbine; a turbine housing was selected which best fit the compressor performance required. The compressor has a 5.06 inch diameter impeller wheel, followed by a vaneless diffuser and scroll collector; the impeller has no backsweep. The radial-inflow turbine has straight radial blades and a conical diffuser exit. The turbine model number is TR 876 BU12, and the compressor model number is ST-50.

3.2 INSTRUMENTATION

The following sections examine the instrumentation used in the determination of the mixing tube length and the compressor characteristic. Also discussed are the high response pressure transducers used to examine the unsteady flow during stall.

3.2.1 Steady-State Instrumentation

To determine the mixing tube length of the air ejector, static pressure taps were placed along the tube length at .65, 5, 6, 7, 8, 9, 10 and 11 diameters downstream from the mixing tube entrance. At the .65 diameter location, four static pressure taps were placed 90^{o} apart and were

used to determine the performance of the convergent-divergent nozzle. The taps at the other locations were placed 180° apart. The diameters 5, 7, 9, and 11 were also provided with Kiel (total pressure) probes positioned so that they were 90° from the static pressure taps at each location.

The secondary stream mass flow was calculated from the average of the four static pressure taps in the inlet with the total pressure being atmospheric. The primary stream mass flow was obtained by using the measured upstream total pressure and temperature and the known area of the throat of the convergent-divergent nozzle, where the flow is choked.

The static pressure of the mixing tube taps was measured with a bank of water manometers. The least scale division was .10 inch and the scale readability was ±.02 inch. The secondary stream mass flow and velocity profile were measured with a manometer tube using oil as the manometer fluid; the manometer fluid has a specific gravity of .827. The primary stream total pressure was measured with a Solfrunt pressure gauge with an accuracy of ±.25 psi.

The turbocharger was instrumented so that the characteristic of the compressor could be determined. The compressor was supplied with thirty static pressure taps and three locations for total pressure measurements. Shown in Figure 10 are the pressure taps along the impeller and vaneless diffuser for one plane of the compressor. At a circumferential position of 180° there are matching static pressure taps. Also shown in Figure 10 is the position of a Cobra probe used to measure the impeller total pressure. The Cobra probe was placed one blade spacing downstream of the impeller.

At the exit of the compressor there are four static pressure taps and two Kiel probes. Static pressure taps were also distributed along the scroll collector. In addition, the total temperature was measured at the

exit using a half-shielded tip thermocouple. This provided measurement of the compressor efficiency from compressor inlet to outlet.

Since the Mach number at compressor exit is low (.27 for the test facility design point), the difference between recovery and stagnation temperature for the thermocouples is small. Also, the temperature of the exit is low enough to make radiation effects insignificant. Thus, use of the half-shielded tip thermocouples should give negligible error (in temperature measurement) due to radiation and convection effects.

The overall compressor characteristic was measured and presented as the variation of corrected mass flow with pressure ratio (total to total) for different corrected rotational speeds. The mass flow and speed were corrected to 14.696 psi and 545°R. The total pressure of the compressor was taken to be the average of the two Kiel probes at the compressor exit.

The turbine was instrumented with a Kiel probe at the entrance and four static pressure taps at the exit of the conical diffuser. This provided the means to measure the expansion ratio (total to static) across the turbine. The total temperature was measured at inlet and exit of the turbine with half-shielded tip thermocouples.

A minicomputer was used to control the measurement of pressure, temperature, rotational speed and reduction of the data; the data acquisition and reduction programs are listed in Appendix C.

A 48 channel Scanivalve was used to gather the pressure data. The output from the Scanivalve is input to the computer through an analog to digital converter. The uncertainty in the pressure measurements was ±.25 psi. This was due to an error in the pressure gauge used to calibrate the pressure transducer in the Scanivalve. In order to reduce this error in the future, a mercury manometer will be used. The listed accuracy of the

transducer is .06% of full scale.

A 12 channel Thermocouple Multiplexer was used to gather the temperature data. The uncertainty in the temperature measurements was found to be $\pm.3^{\circ}C$. The turbocharger RPM was measured through the use of a magnetic pickup and a frequency counter. At 33000 RPM the counter was found to have an error of .5% using a Strobotac to measure RPM. The output from the frequency counter was feed directly into the computer and stored.

The mass flow rate of the compressor was measured using a calibrated inlet. The inlet was calibrated by traversing with a Cobra probe, using an inclined manometer. The least scale division on the inclined manometer was .01 inch and the scale readability was ±.002 inch. The manometer used oil with a specific gravity of .827. The traversing mechanism used a micrometer to read the depth in the inlet pipe; the micrometer could measure to .001 inch.

3.2.2 Dynamic Response Instrumentation

The compressor was also instrumented with dynamic response pressure transducers to diagnose flow phenomena during stall. These pressure transducers have a miniature pressure sensing diaphram of .091 inch diameter (Kulite XT-140-50), and were statically calibrated for a pressure range from 0 to 50 psig and temperature compensated to a maximum temperature of $350^{\circ}F$. They were flush mounted 90° apart along the wall of the compressor at the same axial and radial locations as the static pressure taps shown in Figure 10, but at different circumferential positions. The pressure transducers were positioned at 0° and 90°, and the static pressure taps at 135° and 315°.

The output from these transducers was fed into an interface box, which

amplified the signal. During stall the response of the transducers was input to the analog to digital converter and stored by the computer; the signal was also displayed on a dual trace oscilloscope. A Fast Fourier Transform was performed on the digitized data and plotted out as frequency versus amplitude. Due to disk storage limitations in the present configuration, a maximum of 2048 data points could be taken using two transducers simultaneously at a sample rate of 2.05 kHz. Source listings of the programs are given in Appendix C.

3.3 FACILITY DESCRIPTION

An overall piping diagram of the test facility is shown in Figure 11. During operation air enters the compressor, flows through a valve at the compressor exit (used to control the mass flow), and enters the supply tank. From the supply tank it merges with the high pressure air (from the convergent-divergent nozzle), "mixes out" and enters the turbine. The flow then exits through the laboratory exhaust system (6 inch Steam Ejector) which is used to reduce the turbine exit static pressure.

The turbocharger required an oil supply system for lubrication of the bearings. This system is shown in Figure 12. The oil system had to fulfill the following requirements at the inlet to the bearings: a temperature range between 180^{o}F and 220^{o}F, and a pressure range between 40 psig and 60 psig. Rotella-T 30W motor oil was used as the lubricating fluid.

CHAPTER 4

EXPERIMENTAL RESULTS

4.1 INTRODUCTION

This chapter presents the results of the air ejector modelling, mass flow traverses, and the compressor steady-state characteristic. In addition, some preliminary results of the dynamic pressure measurements of the compressor are discussed.

4.2 AIR EJECTOR MODELLING

As discussed in Section 2.2.5 the air ejector was modelled so that the mixing tube length could be determined experimentally without using the turbocharger. Figure 13 shows the results of the measured mixing tube static pressure versus length. Also shown in this figure are the mass flow ratios corresponding to the three design points selected in the ejector design (Section 2.2.1). This figure shows that the maximum static pressure rise was roughly 7 diameters downstream from the mixing tube entrance for a mass flow ratio of 1.64, but the peak is rather flat.

The velocity profile was also measured and is shown in Figure 14, where the ratio of the velocities (V/V_{CL}) is plotted versus the emersion of the Kiel probe in the mixing tube (Depth/D). This shows the velocity profile at 7 and 9 diameters to be nearly uniform across the pipe signifying that the flow is mixed out. At 5 diameters, however, the profile is not as uniform. Since the maximum static pressure was found to be at 7

diameters, where the flow is nearly uniform across the pipe, this was chosen to be the mixing tube length.

Figures 15 and 16 compare the modelling and design results to experimental measurements. In Figure 15 mixed out Mach number is plotted versus the ratio of the primary to secondary stream mass flow rates. This figure shows the experimental points being almost coincident with the modelling results. The slightly higher Mach numbers determined experimentally were due to the boundary layer growth in the mixing tube, which reduced the effective area.

The difference between the modelling results and the design points is caused by the assumption of equal total temperatures for the primary and secondary stream used in the modelling. If the total temperatures were taken as equal in the design analysis, the design points are coincident with the modelling results.

In Figure 16 the mass flow ratio is plotted versus the ratio of the primary stream total pressure to mixed out total pressure. As can be seen, the experimental results lie above the modelling curve indicating a smaller pressure rise. This is due to wall friction in the mixing tube. The design points are found to lie below the modelling curve indicating a slightly higher pressure gain due again to the differences in inlet total temperatures.

In addition, the Mach number of the primary stream was measured for each mass flow ratio corresponding to the design points and found to be 1.62.

4.3 STEAM EJECTOR

Due to the lack of documentation, experimental tests had to be performed on the laboratory exhaust system (Steam Ejector) to find out if the system could reduce the turbine exit static pressure enough to drive the compressor at the test facility design point. The characteristic was measured with use of a bellmouth inlet attached to a valve leading to the exhaust system. As the valve was opened, the mass flow was measured using the average of four static pressure taps in the inlet. The performance was measured with and without a fairly high solidity screen following the inlet to provide system resistance. The Steam Ejector static pressure was measured downstream of the screen position in both cases.

The characteristic of the Steam Ejector, with and without the screen, is shown in Figure 17, where the performance is plotted as corrected mass flow versus the ratio of the static pressure to atmospheric pressure. The mass flow was corrected to $545^{\circ}R$ and 14.696 psi. Also shown in this figure is the required performance of the Steam Ejector to drive the compressor at the test facility design point. The operating range of the Steam Ejector lies between the curves denoted "screen" and "no screen"; the operating range would vary if a different type of screen was used (different solidity). As can be seen the test facility design point is within the operating range. Thus the Steam Ejector was able to achieve the level of back pressure reduction needed to drive the compressor at the test facility design point, and this meant that heating of the air to increase turbine work could be eliminated.

4.4 INLET CALIBRATION

The compressor inlet consisted of a 4.375 inch diameter 2 foot long tube with a bellmouth inlet leading to the inducer portion of the impeller. The mass flow entering the compressor was calculated from the static pressures measured six inches downstream of the tube entrance. To correct for inlet boundary layer, an effective area was used (tube area minus the displacement thickness). This was determined by measuring the boundary layer six inches downstream of the inlet tube entrance and calculating the displacement thickness. Over the range of mass flows for which the compressor had stable flow, the effective area was found to be .99 of the actual area and was kept as constant in our flow calculations.

4.5 COMPRESSOR STEADY-STATE CHARACTERISTIC

A prerequisite to any compressor instability investigation is the measurement of the compressor's steady-state performance map. Centrifugal compressor performance maps are generally presented as corrected mass flow versus total to total pressure ratio for different constant corrected rotational speeds (usually referred to as speedlines). On a line of constant speed, as the flow through the compressor is decreased, a line is reached which separates stable operation from unstable operation. This line is often defined as the "surge" line, and steady flow is generally not possible to the left of this line.

Results of the determination of the overall performance map of the compressor used in this investigation is shown in Figure 18, which gives the variation of corrected mass flow with pressure ratio (total to total) for four different corrected speeds: nominally 33000, 39000, 45000, and 51000 RPM. The line separating the stable and the unstable operating

regions of the compressor characteristic is also shown.

Due to mass flow limitations inherent in the present facility, the available stable mass flow range of the compressor decreases as the rotational speed increases. Over and above this, however, there is a marked change in stall point as a function of speed. This is most dramatic between the speedlines of 39k and 45k RPM where the stable mass flow range decreases sharply. At the lower rotational speeds (33k and 39k RPM), the pressure ratio rose slightly from the maximum flow obtainable with the test facility to a flat region which was obtained over a substantial portion of the flow range. As the flow was decreased further the pressure ratio decreased gradually until the surge line was reached. Since there is a maximum flow and pressure ratio limit, only part of the speedline at the higher speeds can be obtained. Thus, at the highest speed measured (51k RPM), the pressure ratio decreased from the maximum flow measured to the surge line. At 45k RPM, the pressure ratio reached a peak with decreasing flow and then dropped gradually until the surge line was encountered. The experimental uncertainties in mass flow for the various speedlines at the stall point are: ±1.90% at 33k RPM, ±.85% at 39k RPM, ±.20% at 45k RPM, and ±.16% at 51k RPM.

Figure 19 shows the same overall characteristic, but this time it is presented as the variation of axial velocity (nondimensionalized by the inducer tip speed) with pressure ratio (total to total) for the same four speedlines. The nondimensional parameter, C_x/U, gives a measure of the relative inlet flow angle at the inducer inlet. Notice at the high speeds (51k and 45k RPM) the compressor surged at the same value of C_x/U.

One difficulty encountered in this investigation was the determination of the surge line, or point for the individual speedlines. The variation

in the point (C_x/U) at which each speedline surged is given in Table 3, along with the maximum percent difference. As can be seen, the greatest variation occurred at the 45k RPM speedline where the difference in the surge point between two different runs is 73%. The minimum variation occurred at 51k RPM, where there is no difference between the separate runs.

The differences in the point of instability from run to run is believed to be caused by the procedure used to throttle the compressor. This procedure varied according to the speedline desired and the other users on the high pressure laboratory air supply. Although some discussion of this point is given below, it is planned to document this in more detail during the next phase of the tests.

For speedlines below 45k RPM, the Steam Ejector was used to obtain the maximum flow point through the compressor with the valve to the laboratory air supply closed. The turbine exit pressure was then increased by slightly closing the Steam Ejector valve. The valve to the laboratory air supply was adjusted and the test facility is now being used in its air ejector configuration. This procedure was repeated over a substantial portion of the speedline. When the turbine exit pressure approached atmospheric, the compressor was further throttled (towards surge) by using a valve located at the compressor exit. By following this procedure, steady rotational speeds were attainable as the surge line was approached.

For speedlines of 45k RPM and above, the Steam Ejector alone could not be used to obtain the maximum flow point, making it necessary to use the laboratory air supply as well. From this point on, the same procedure was used as for speedlines below 45k RPM.

The procedures outlined above were used when no other users required

the laboratory air supply. However, on those runs when the air supply was in great demand, the compressor exit valve was used extensively to throttle the compressor. The amount of throttling required of the compressor exit valve thus depended upon the other users' requirements of the laboratory air supply and it was found that this could cause large variations in the stall point between runs.

Since the compressor characteristic should be the same for different runs, the difference in the flow through area of the valve (amount of throttling) is the most likely cause of the variation in surge point between runs. This can be better understood from consideration of the dynamic stability of the compression system. For small perturbations from the mean flow, dynamic instability can occur when the net mechanical energy output from the compressor is greater than during mean (steady) flow. When the net energy input balances the net dissipation over a cycle, a periodic oscillation can be maintained [15]. This situation exists only when the compressor is operating on the positively sloped portion of the characteristic.

On those runs where extensive throttling was done with the compressor exit valve, the compressor surged at a higher C_x/U (see Table 3). On these runs the situation may therefore be that the different amount of throttling has already affected the dynamic stability of the compression system. This should be examined further by performing specific tests to document the dependency of surge point on throttling.

4.6 DYNAMIC RESPONSE PRESSURE MEASUREMENTS

In order to determine the flow behavior preceding and during stall, the centrifugal compressor was equipped with dynamic response pressure

transducers. From measurements taken with these transducers it is hoped that questions such as those presented in the introduction can be addressed.

The results described below are for the 51k RPM speedline. Two pressure transducers were placed in the compressor for these measurements: one over the axial inducer portion of the impeller (channel 2), and the other, 90° circumferentially and in front of the inducer (channel 1). Only two transducers could be used at the time of this study. At present, however, two more channels are being added to the interface box so that four pressure transducers can be used at the same time. This will allow measurements to be taken at two separate axial or radial positions in the centrifugal compressor.

The response of the pressure transducers was resolved in the frequency domain to see if there was a predominant frequency lower than the blade passing frequency (one per rev). This would indicate a rotating stall or, for extremely low frequencies, a system surge. In Figures 20 through 26, the variation of frequency with amplitude is shown. Also, shown are the values of C_x/U at which the data was taken as the compressor was throttled down the steady-state characteristic.

At a C_x/U of .34 the first data point was taken and is shown in Figure 20. As can be seen there is a large amplitude spike at the blade passing frequency and a smaller amplitude spike at 94 Hz. (The blade passing frequency measured in this figure is 2.54% below that measured by the frequency counter indicating that there is an error in the frequency counter's measurement of rotational speed.) This lower frequency point could be a rotating stall. If this is true, the stall cell is rotating around the annulus at 11% of the impeller rotational speed.

As the compressor was further throttled (C_x/U of .30) the smaller amplitude spike keeps roughly the same amplitude but has an increase in frequency to 199 Hz (Figure 21). This is 24% of the compressor rotational speed. At a C_x/U of .27 (Figure 22), the amplitude of the low frequency spike has increased and is higher than the blade passing frequency. The frequency has also increased to 233 Hz, or 28% of the blade speed. In addition, this figure shows a spike at a lower frequency (28 Hz) than the possible rotating stall frequency (233 Hz).

The 28 Hz frequency spike grows in amplitude as the compressor is throttled to a C_x/U of .26 (Figure 23). There is also a large amplitude spike at 224 Hz which is 27% of the compressor rotational speed.

Figure 24 shows the results when the compressor encountered surge. As can be seen, the 28 Hz frequency has the highest amplitude. This is the surge frequency which was shown to grow in amplitude as the compressor was throttled toward the surge point. Also, shown is a spike at 269 Hz which is approximately 32% of the rotational speed. This seems to indicate that the compressor is going in and out of surge with a rotating stall region preceding or following the surge.

Bammert and Rautenberg [4] have examined a centrifugal compressor in surge. They found a cyclic behavior with a cycle that lasted approximately 7 seconds. The important point is that after a period of low frequency high amplitude fluctuation, the pressure versus time results show that there was a period of time in which the compressor operated in rotating stall. Following this, there was a recovery period and the cycle was repeated.

In order to verify that the compressor was in rotating stall pressure versus time plots were obtained of the data. These results are shown in

Figures 25 and 26 for C_x/U of .30 and .26, respectively. As can be seen in Figure 25, there is no clear indication that the compressor is in a rotating stall, but Figure 26 seems to show that there is a rotating stall in the impeller region. However, the sampling rate used was such that only 2 data points were taken per revolution of the compressor (due to limitations of the current computer configuration being used). In order to resolve if a rotating stall is actually present, the number of points per revolution should be increased.

A plot of the variation of pressure with time to the left of the surge line is given in Figure 27. This figure shows two complete cycles of system surge. During each surge cycle, large amplitude fluctuations in pressure with smaller variations in pressure superimposed upon them are shown. The smaller pressure fluctuations could be the result of rotating stall occurring within each surge cycle.

The above preliminary results of dynamic response pressure measurements at 51k RPM imply that as the surge point is approached, rotating stall exists in the impeller and grows in rotational speed and amplitude of disturbance. Close to the surge line, the surge frequency appears and grows in magnitude until the surge point is reached, where it is the predominant frequency.

Although other data has been obtained at different speedlines, this should be regarded as of a preliminary nature. The results indicate that in the future, all four probes should be placed in the compressor at the same time. Also, the number of data points per revolution should be increased in order to obtain verification of presence of rotating stall in the impeller of the compressor.

CHAPTER 5

CONCLUSIONS AND RECOMMENDATIONS

5.1 SUMMARY AND CONCLUSIONS

The main emphasis of this investigation was the design and construction of a turbocharger test facility and the instrumentation of the centrifugal compressor. The test facility was designed so the centrifugal compressor would operate at a pressure ratio of 2.0 and a mass flow of 50 LBm/min.

To accomplish this goal, an air ejection system was designed using the Gas Turbine Laboratory high pressure air supply and the compressor exhaust flow. In order to increase the expansion ratio, the Gas Turbine Laboratory exhaust system (Steam Ejector) was used to decrease the turbine exit pressure below atmospheric. This allowed the turbine to produce enough work for the compressor to operate at the test facility design point. The facility is now working and appears to be reasonably convenient to operate with good reproducibility.

The compressor was equiped with steady-state as well as dynamic response instrumentation. An overall performance map was obtained for the compressor, and dynamic response pressure measurements taken. The overall performance of the compressor was measured at four different rotational speeds. The stall points were found to depend upon the amount of throttling done by the valve at the compressor exit. Thus further

investigation is required to clearly define the stall point of the different speedlines.

Dynamic response pressure measurements were taken in the inducer region of the compressor at a rotational speed of 51k RPM. It was found that rotating stall may be present in the impeller preceding system surge. As the compressor was throttled towards surge the amplitude and frequency of this "rotating stall" increased. In addition, as surge was approached the surge frequency was observed to grow in amplitude. At the stall line, the surge frequency predominated and was found to be 28 Hz.

5.2 RECOMMENDATIONS

The present work is only the preliminary phase of an ongoing project. The test facility constructed was found to be able to run the centrifugal compressor over a substantial flow range. However, certain improvements on the facility should be made.

When running at high speeds (above 39k RPM) the oil was found to reach its upper temperature range ($220^{o}F$) quite rapidly. In order to keep the oil temperature within the operating range, a heat exchanger should be added to the oil system. Also, use of flexible hose with higher pressure and temperature ranges will allow the facility to operate at compressor rotational speeds in excess of 51k RPM.

For the dynamic response measurements, four transducers should be used simultaneously. In addition, a high frequency filter should be used, since frequency below the one per revolution are of interest. Also, as discussed previously, the number of points taken per revolution should be increased to document whether the impeller is in rotating stall.

The magnetic pick-up used in this investigation had an output voltage

which was below the threshold voltage of the frequency counter. Thus, in order to measure the rotational speed, the output from the pick-up had to be amplified before being input to the counter. The electrical noise level of the amplifier was such that the counter picked up spurious signals. (This was apparent in the dynamic response pressure measurements which were resolved in the frequency domain.) At low speeds the counter was found to indicate a rotational speed higher than the actual speed. Therefore, a better amplifier should be obtained, or a magnetic pick-up with a higher output voltage (above the threshold of the counter) should be used.

For the steady-state measurements, the Cobra probe should be placed in the compressor at the location shown in Figure 10. This will allow determination of the impeller and the vaneless diffuser characteristics and might give some indication of which component causes the centrifugal compressor to stall. Finally, as stated in Chapter 4, the dependence of the surge point on throttling should be addressed.

REFERENCES

1. Abdelhamid, A. N., "Effects of Vaneless Diffuser Geometry on Flow Instability in Centrifugal Compression Systems," ASME Paper No. 81-GT-10, 1981.

2. Addy, A. L., "The Analysis of Supersonic Ejector Systems," AGARD-AG-163, Ed. J. J. Ginoux, 1972.

3. Amann, C. A. and Nordenson, G. E., "The Role of the Compressor in Limiting Automotive Gas Turbine Acceleration," Centrifugal Compressors, Technical Progress Series Vol. 3, ASME, New York, 1961, p. 74.

4. Bammert, K. and Rautenberg, M., "An Analysis of the Non-Steady and Non-Stable Flow Mechanisms in a Radial Compressor Impeller," ASME Paper No. 77-WA/GT, 1977.

5. Benedict, R. P., Carlucci, N. A. and Swetz, S. D., "Flow Losses in Abrupt Enlargements and Contractions," ASME Journal of Engineering for Power, Vol. 88, Jan. 1966, p. 73-81.

6. Day, I. J., Greitzer, E. M., and Cumpsty, N. A., "Prediction of Compressor Performance in Rotating Stall," ASME Journal of Engineering for Power, Vol. 100, Jan. 1978, pp. 1-14.

7. Dean, R. C., "The Centrifugal Compressor," Creare, Inc., Technical Note TN-183, 1973.

8. Dean, R. C., Jr., and Young, L. R., "The Time Domain of Centrifugal Compressor and Pump Stability and Surge," in Centrifugal Compressor and Pump Stability, Stall and Surge, eds. P. C. Tramm and R. C. Dean, Jr. (New York: The American Society of Mechanical Engineers, 1976), pp. 91-106.

9. Emmons, H. W., Pearson, C. E., and Grant, H. P., "Compressor Surge and Stall Propagation," Trans. ASME Vol. 77, Apr. 1955, p. 455-469.

10. Flynn, P. F. and Weber, H. G., "Design and Test of an Extremely Wide Flow Range Compressor," ASME Paper No. 79-Gt-80, 1979.

11. Foelsch, Kuno, "The Analytical Design of an Axially Symmetric Laval Nozzle for a Parallel and Uniform Jet," Journal of Aeronautical Science, Vol. 16, 1949, pp. 161-188.

12. Greitzer, E. M., "Review - Axial Compressor Stall Phenomena," ASME Journal of Fluids Engineering, Vol. 102, 1980, pp. 162-168.

13. Greitzer, E. M., "Surge and Rotating Stall in Axial Flow Compressors, Part I: Theoretical Compression System Model," ASME Journal of Engineering for Power, Vol. 98, Apr. 1976, pp. 190-198.

14. Greitzer, E. M., "Surge and Rotating Stall in Axial Flow Compressors, Part II: Experimental Results and Comparison with Theory," ASME Journal of Engineering for Power, Vol. 98, Apr. 1976, pp. 199-217.

15. Greitzer, E. M., "The Stability of Pumping Systems - The 1980 Freeman Scholar Lecture," ASME Journal of Fluids Engineering, Vol. 103, 1981, pp. 193-242.

16. Hansen, K. E., Jorgensen, P. and Larsen, P. S., "Experimental and Theoretical Study of Surge in a Small Centrifugal Compressor," ASME Journal of Fluids Engineering, Vol. 103, 1981, pp. 391-395.

17. Hopkins, D. F. and D. E. Hill, "Effect of Small Radius of Curvature on Transonic Flow in Axisymmetric Nozzles," AIAA Journal, Vol. 4, no. 8, 1966, pp. 1337-1343.

18. Horlock, J. H., Axial Flow Compressors Fluid Mechanics and Thermodynamics, (New York: Robert E. Krieger Publ. Co. 1973).

19. Jansen, W., Carter, A. F., and Swarden, M. C., "Improvements in Surge Margin for Centrifugal Compressors," in Centrifugal Compressors, Flow Phenomena and Performance, AGARD Conference Proceedings No. 282, 1980, Reference 19.

20. Kammer, N. and Rautenberg, M., "An Experimental Investigation of Rotating Stall Flow in a Centrifugal Compressor," ASME Report No. 82-GT-82, 1982.

21. Keenan, J. H. and E. P. Neumann, "A Simple Air Ejector," Journal of Applied Mechanics, Trans. ASME, Vol. 64, 1942, pp. A-75-A-84.

22. Keenan, J. H., E. P. Neumann, and F. Lustwerk, "An Investigation of Ejector Design by Analysis and Experiment," Journal of Applied Mechanics, Vol. 17, September 1950, pp. 299-309.

23. Liepmann, H. W. and Roshko, A., Elements of Gas Dynamics, (New York: John Wiley and Sons, Inc., 1957).

24. Morel, T., "Comprehensive Design of Axisymmetric Wind Tunnel Contractions," ASME Journal of Fluids Engineering, Vol. 97, 1975, pp. 225-233.

25. Olson, A. T., "Nozzle Discharge Coefficients-Compressible Flow," ASME Journal of Fluids Engineering, Vol. 94, Mar. 1974, pp. 21-24.

26. Otis, D. R., "Choking and Mixing of Two Compressible Fluid Streams," ASME Journal of Fluids Engineering, Vol. 98, June 1976, pp. 311-317.

27. Pampreen, R. C., "A Blockage Model for Centrifugal Compressor Impellers," ASME Report No. 81-GT-11, 1981.

28. Puckett, A. E., "Supersonic Nozzle Design," Journal of Applied Mechanics, Vol. 13, 1946, pp. A-265-A-270.

29. Sauer, R., "General Characteristics of the Flow through Nozzles at Near Critical Speeds," NACA TM No. 1147, 1947.

30. Sissom, L. E. and Pitts, D. R., Elements of Transport Phenomena, (New York: McGraw-Hill Book Co., 1972).

31. Smith, R. H. and Chi-Teh Wang, "Contracting Cones Giving Uniform Throat Speeds," Journal of Aeronautical Science, Vol. 11, 1944, pp. 356-360.

32. Stenning, A. H., "Rotating Stall and Surge," ASME Journal of Fluids Engineering, Vol. 102, Mar. 1980, p.14-20.

33. Szczeniowski, B., "Contraction Cone for a Wind Tunnel," Journal of Aeronautical Science, Vol. 10, 1943, pp. 311-312.

34. Taylor, E. S., "The Centrifugal Compressor," Aerodynamics of Turbines and Compressors, (New Jersey: Princeton University Press, 1964), p. 573.

35. Toyama, K., Runstadler, P. W., and Dean, R. C., "An Experimental Study of Surge in Centrifugal Compressors," in Centrifugal Compressor and Pump Stability, Stall and Surge, eds. P. C. Tramm and R. C. Dean, Jr. (New York: The American Society of Mechanical Engineers, 1976), pp. 37-68.

36. Tsien, H., "The Design of the Contraction Cone for a Wind Tunnel," Journal of Aeronautical Science, Vol. 10, 1943, pp. 68-70.

37. Uebelhack, H. T., "One-Dimensional Inviscid Analysis of Supersonic Ejectors," AGARD-AG-163, Ed. J. J. Ginoux, 1972.

38. Weatherston, R., "Mixing of Any Number of Streams in a Duct of Constant Cross-Sectional Area," Journal of Aeronautical Science, Nov. 1949, pp. 697-704.

39. Whitfield, A. and Roberts, D. V., The Effect of Impeller Tip Design on the Performance of a Mixed Flow Turbocharger Compressor," ASME Paper No. 81-GT-7, 1981.

40. Yu, Ying-Nien, "A Summary of Design Techniques for Axisymmetric Hypersonic Wind Tunnels," AGARD-AG-35, 1958, pp. 8-25.

Table 1. Optimum Conditions for the Air Ejection System

Pipe Nominal Diameter = 3 in

$\dot{m}_o$(LBm/min)	$\dot{m}_i$(LBm/min)	M_i	P_{T2}(psi)	$\dot{m}_2$(LBm/min)
40	30	1.61	32.9	70
45	30	1.62	33.0	75
50	30	1.62	33.1	80

$(A_i)_{EXIT}$ = 0.221 in^2

Table 2. Summary of Modelling of Ejector

DESIGN POINTS			MODEL POINTS		
P_{Ti}/P_{T2}	$\dot{m}_o/\dot{m}_i$	M_2	P_{Ti}/P_{T2}	$\dot{m}_o/\dot{m}_i$	M_2
3.79	1.33	.131	3.93	1.35	.127
3.78	1.50	.141	3.93	1.50	.136
3.78	1.66	.151	3.93	1.66	.144

Table 3. Variation of the Compressor Stall Line

Corrected Speed	Run Number	C_x/U	Maximum Percent Difference
51000	14	.26	0
51000	20	.26	
45000	12	.15	73
45000	18	.26	
39000	10	.14	7.14
39000	19	.15	
33000	11	.13	
33000	15	.11	18.2
33000	21	.12	

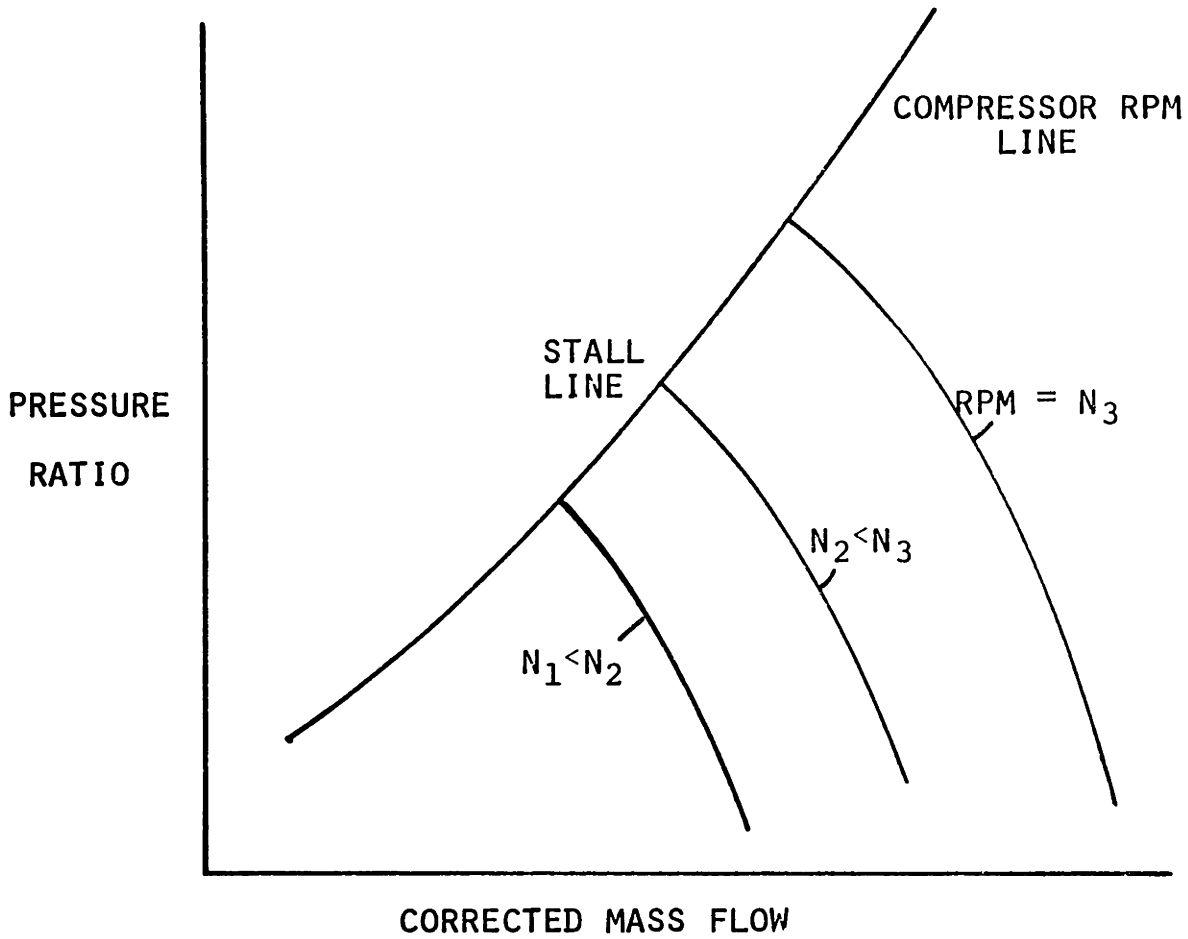

FIGURE 1: COMPRESSOR PERFORMANCE MAP

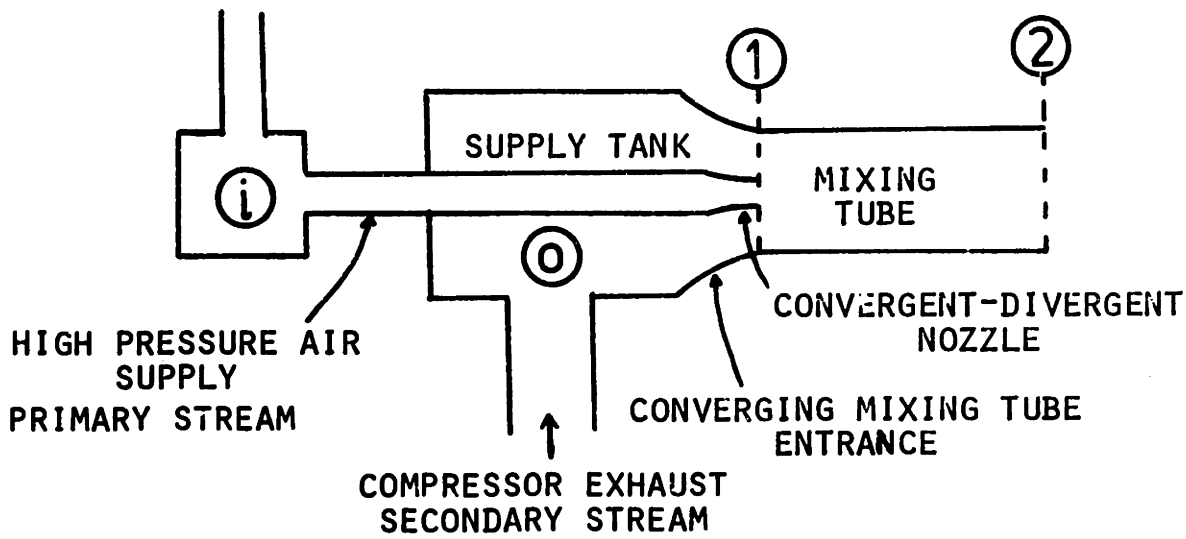

FIGURE 2: SIMPLE AIR EJECTOR

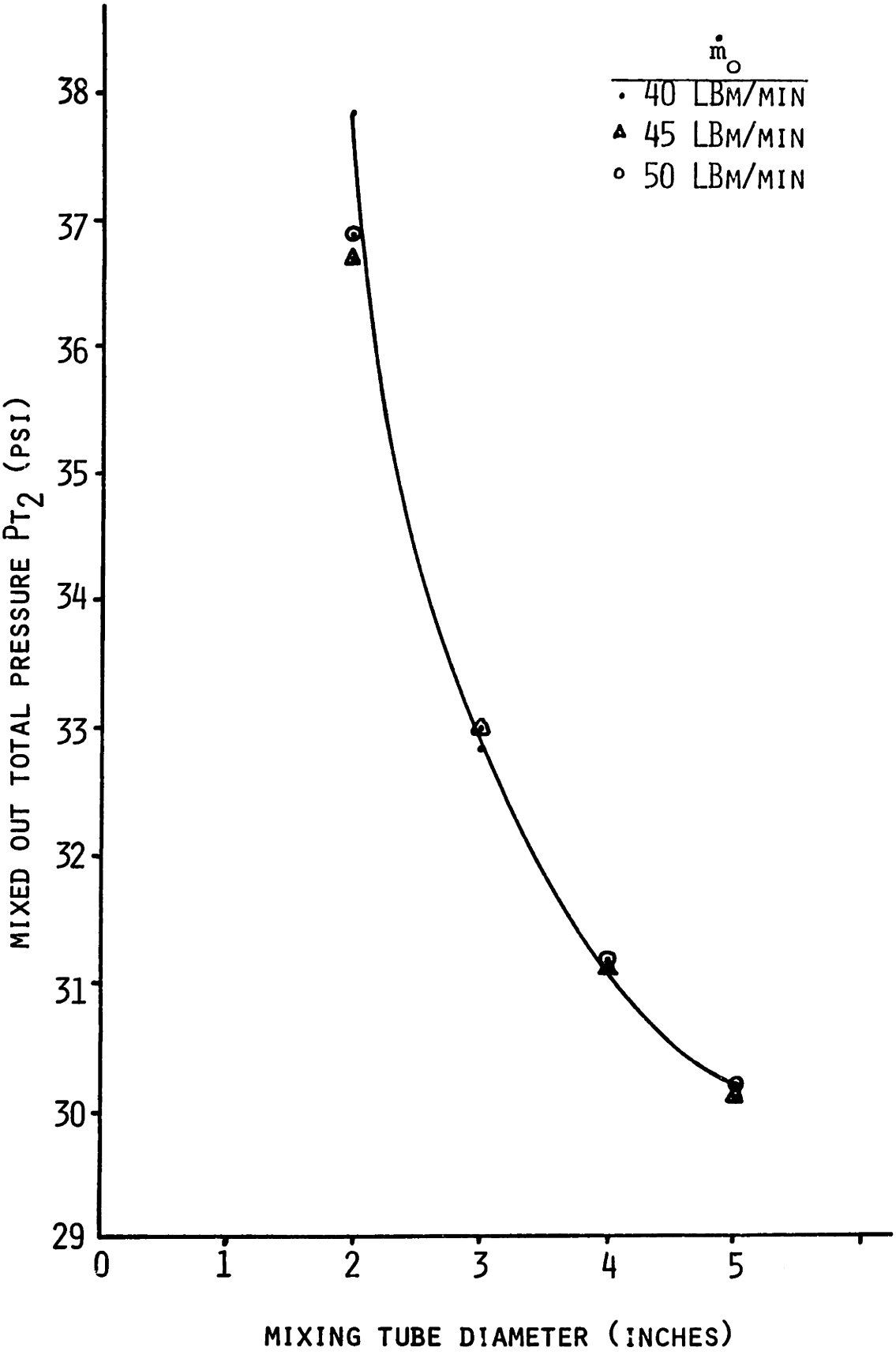

FIGURE 3. AIR EJECTOR RESULTS FOR P_{T_i} = 75 PSI

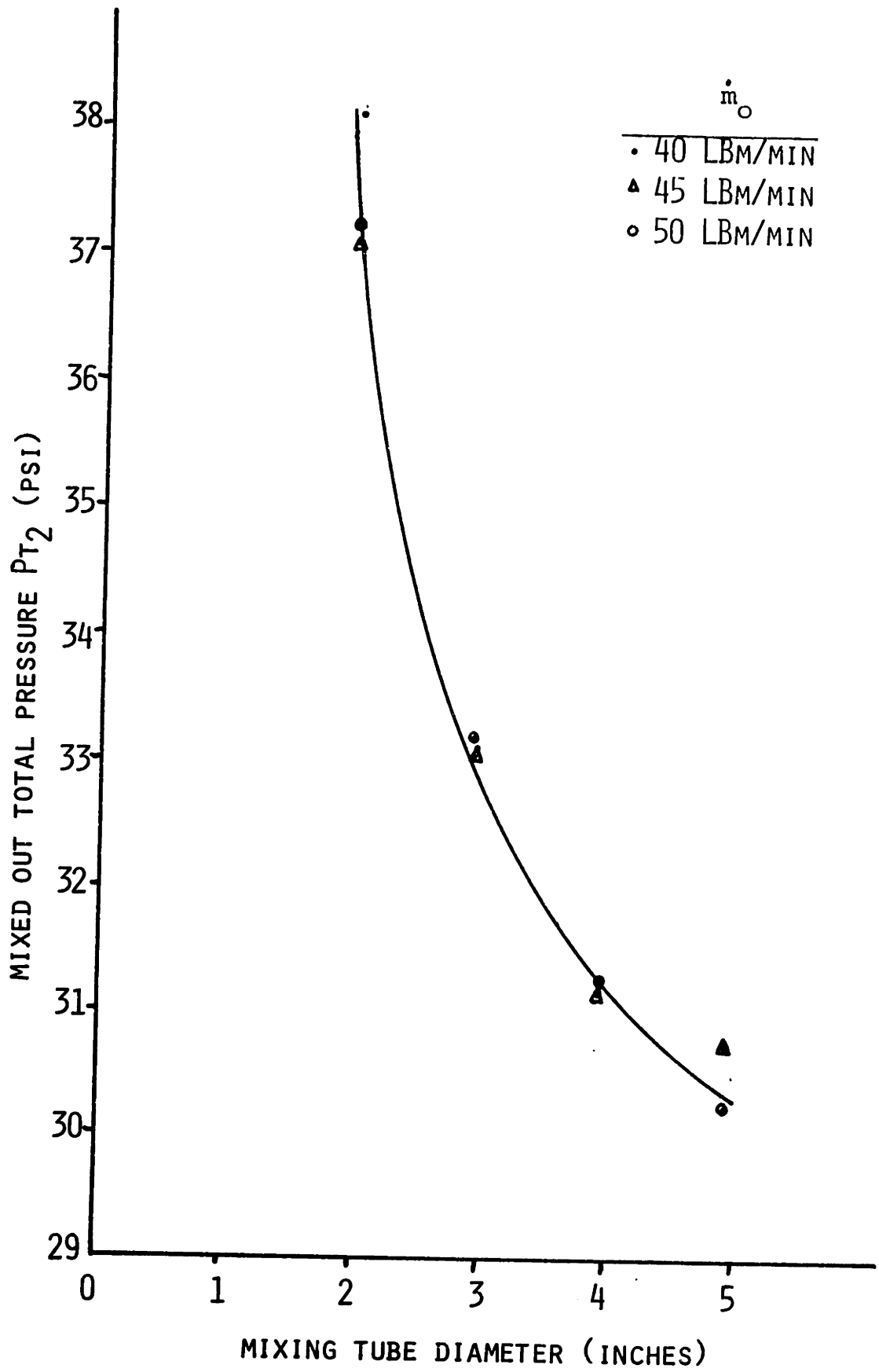

FIGURE 4. AIR EJECTOR RESULTS FOR P_{T_i} = 100 PSI

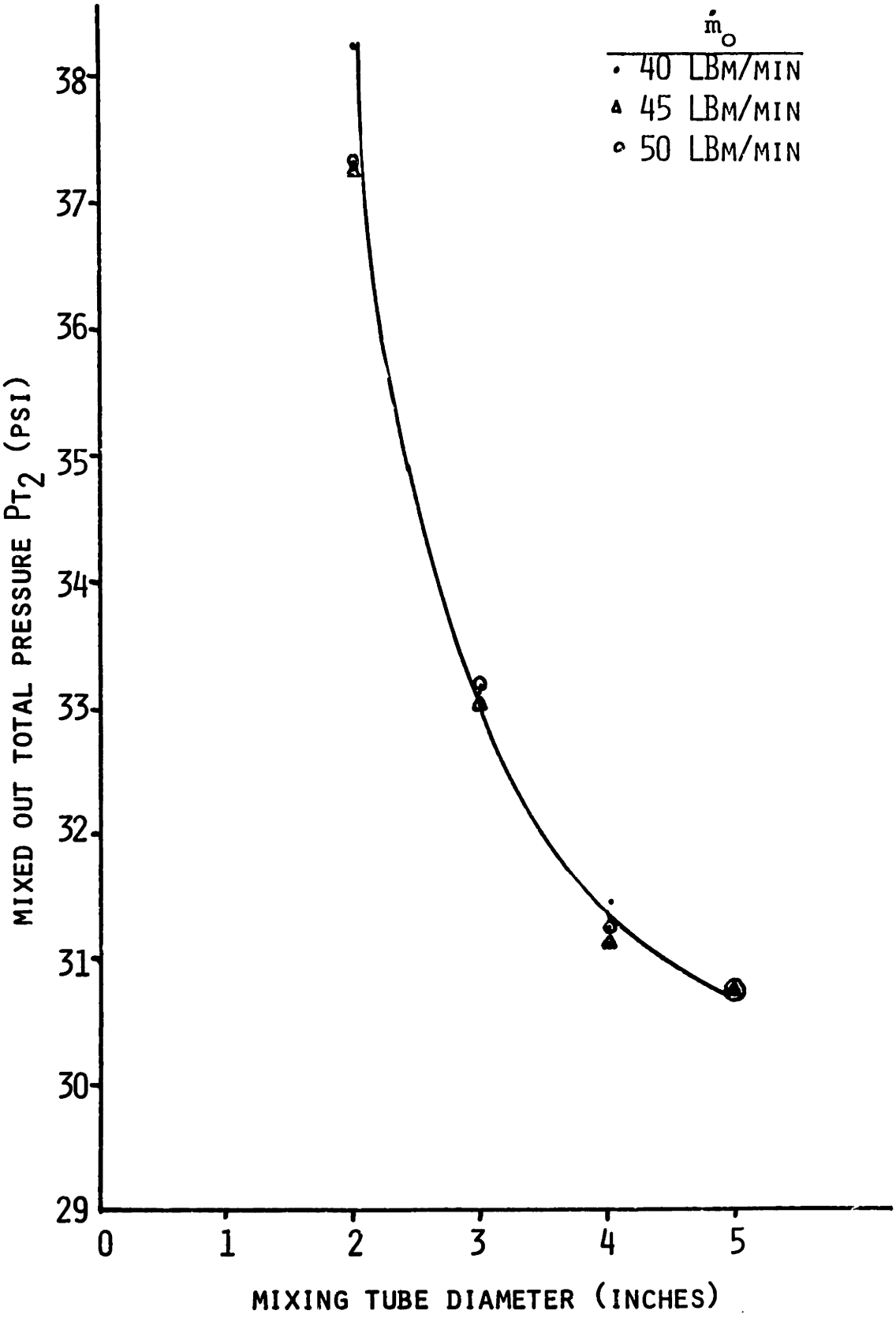

FIGURE 5. AIR EJECTOR RESULTS FOR P_{T_i} = 125 PSI

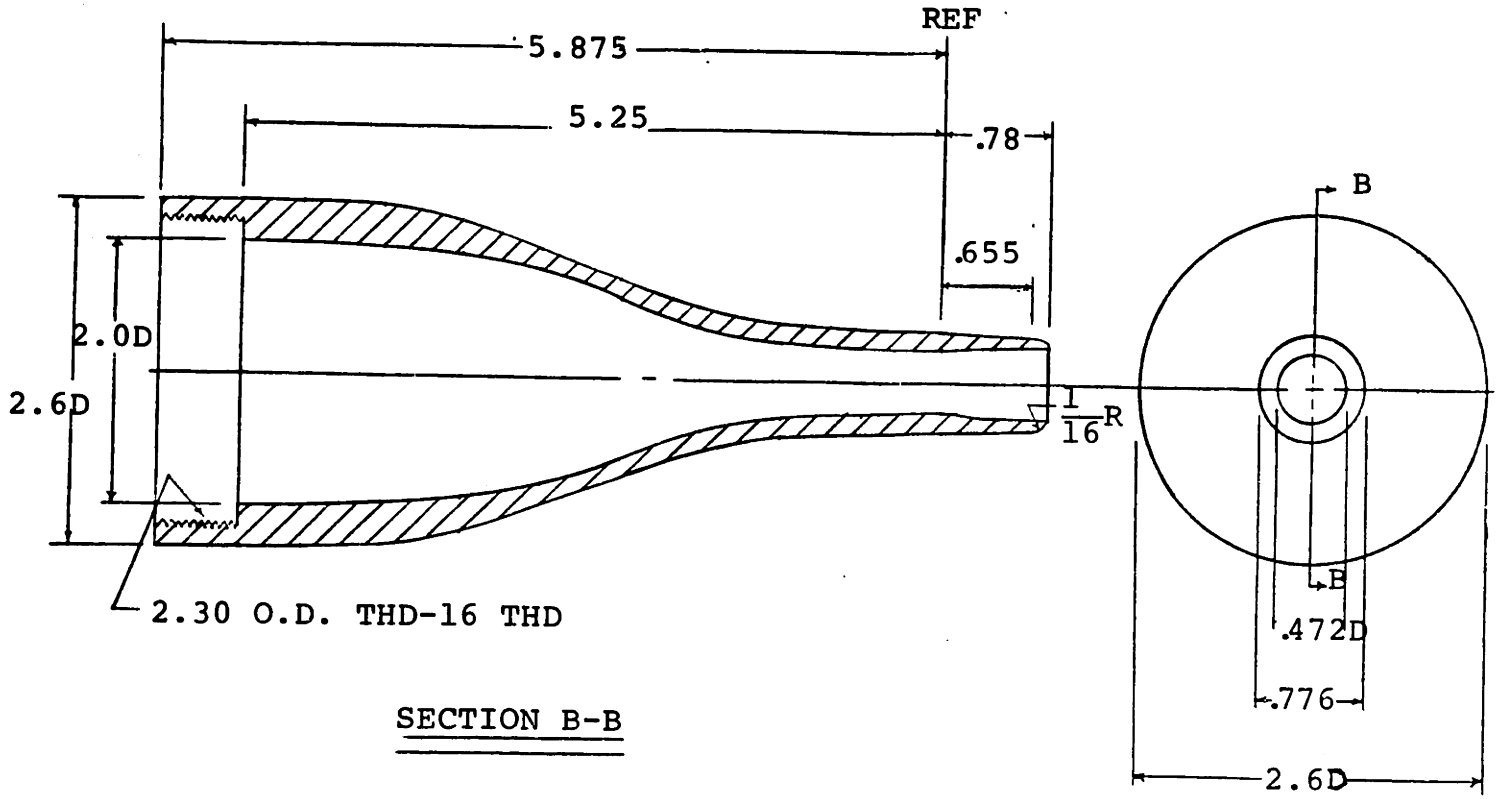

MATERIAL: ALUMINUM
ALL DIMENSIONS IN INCHES

FIGURE 6. CONVERGENT-DIVERGENT NOZZLE DESIGN

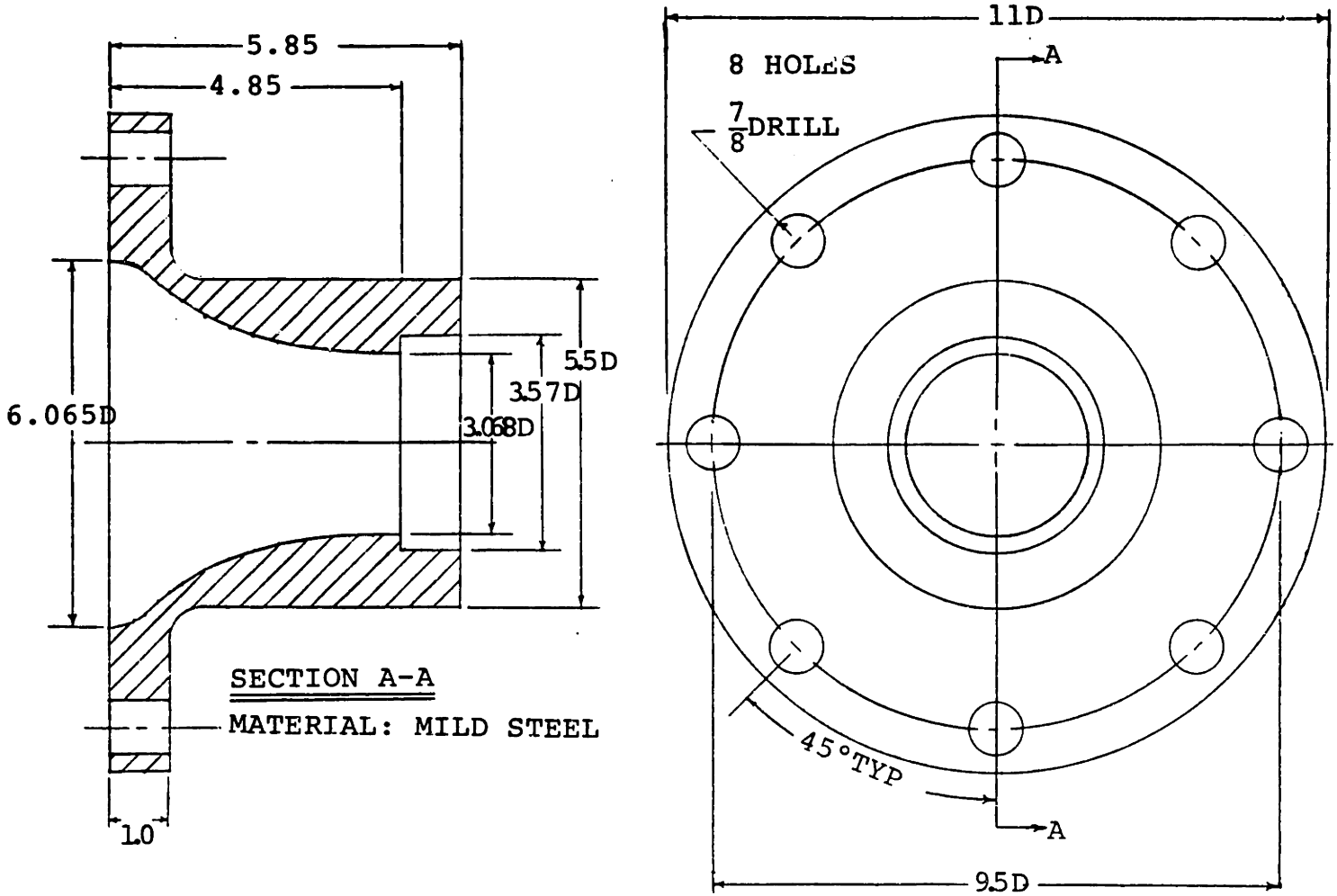

FIGURE 7. MIXING TUBE ENTRANCE (ALL DIMENSIONS IN INCHES)

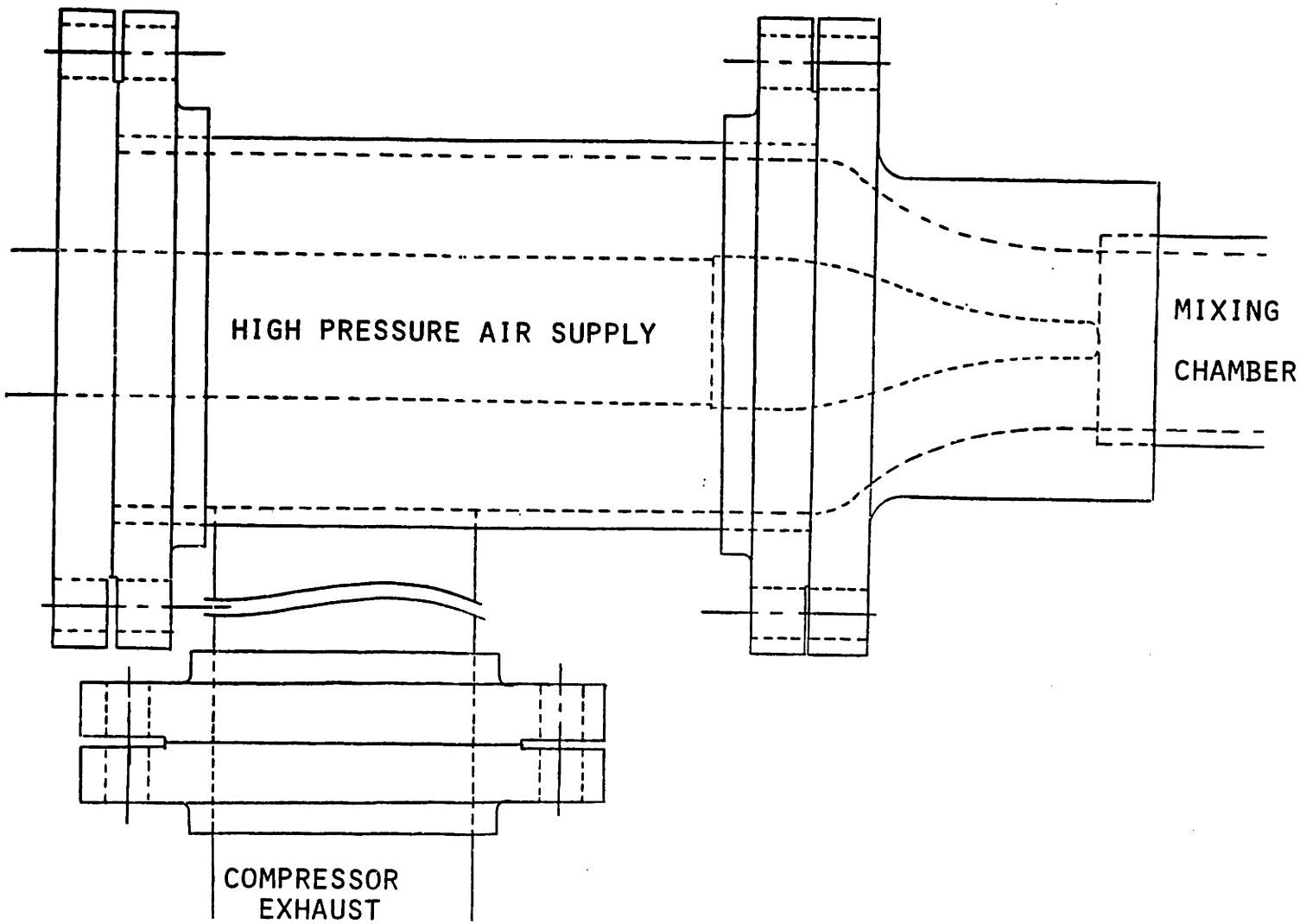

FIGURE 8. AIR EJECTION SYSTEM

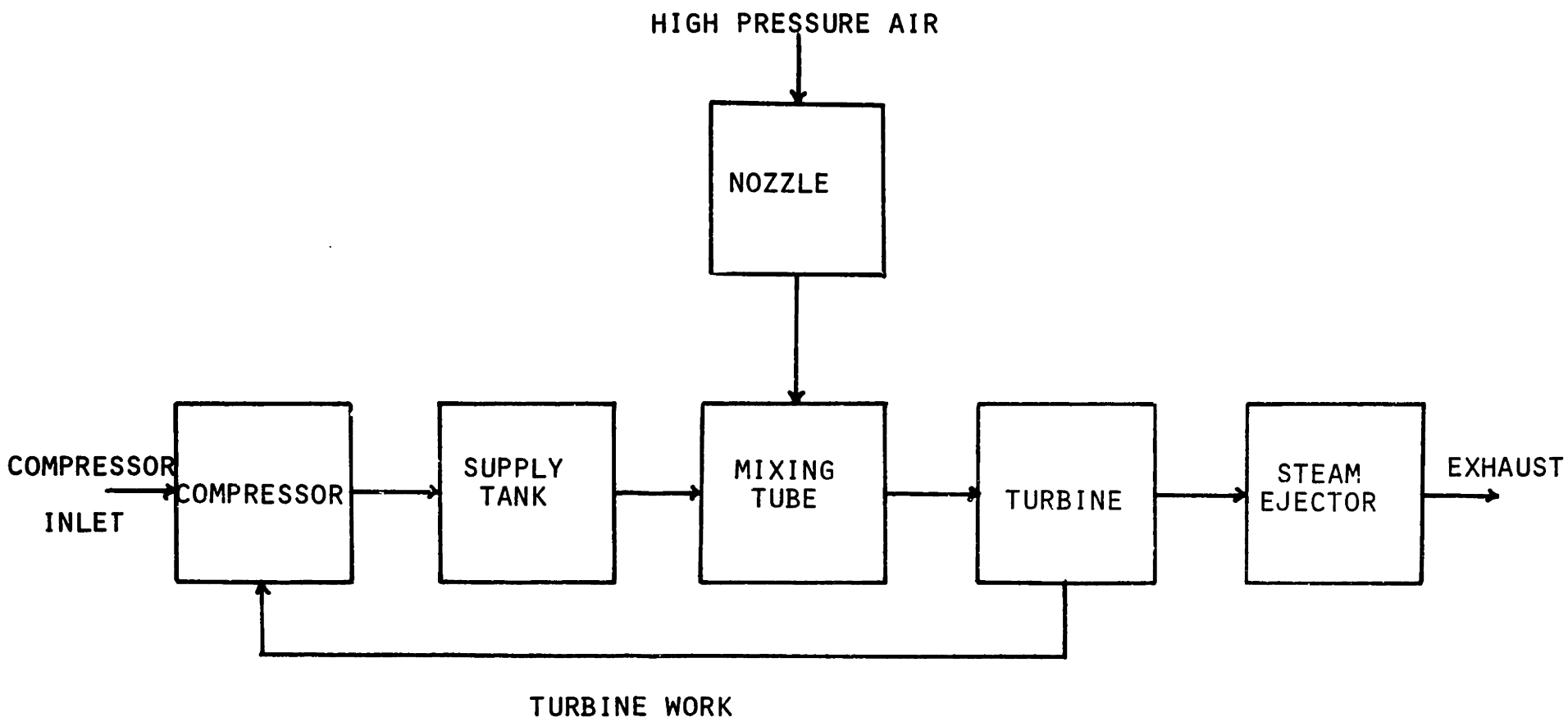

FIGURE 9. SYSTEM DIAGRAM

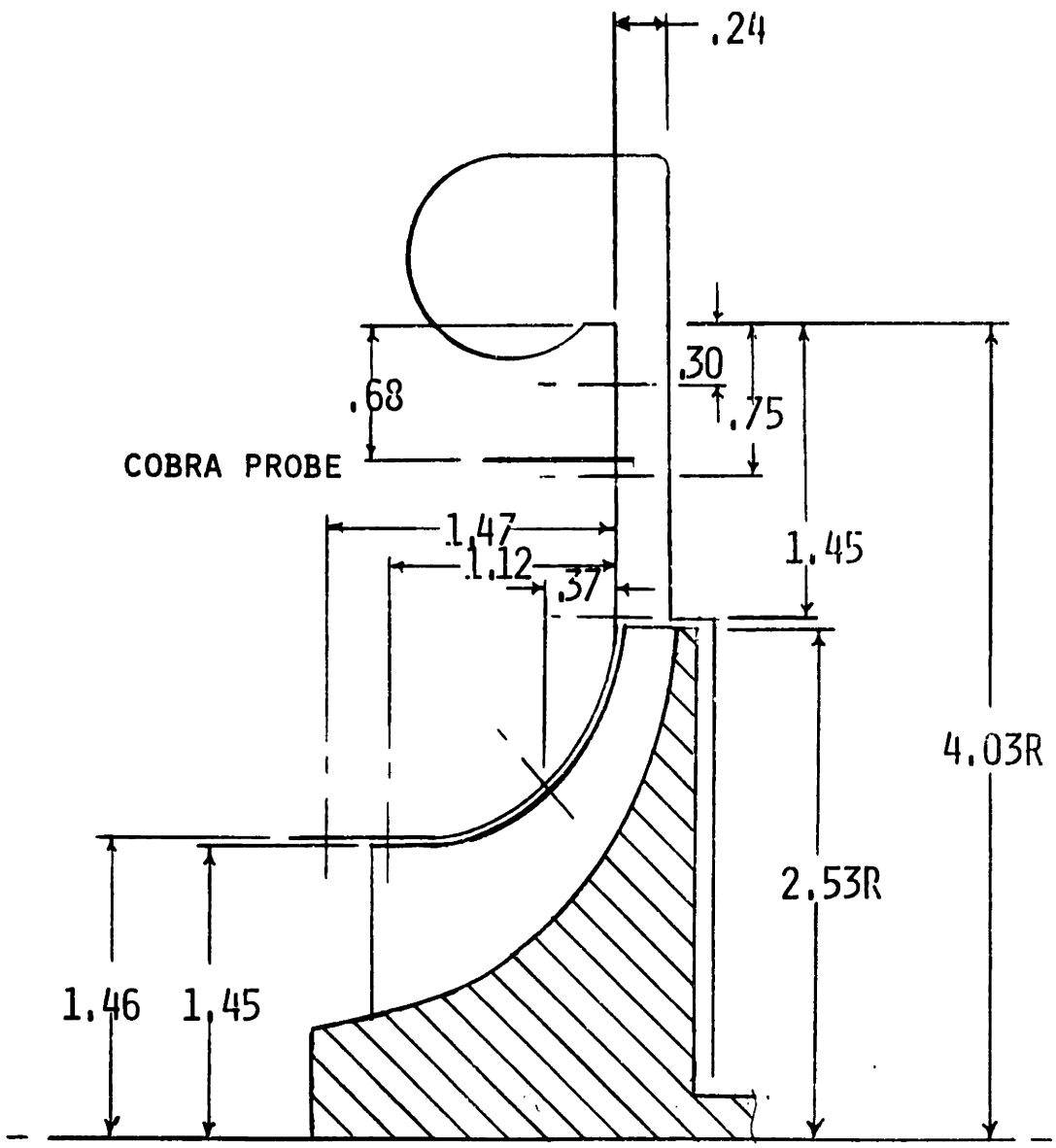

FIGURE 10. LOCATION OF STATIC PRESSURE TAPS AND DYNAMIC RESPONSE PRESSURE TRANSDUCERS

FIGURE 11. OVERALL PIPING DIAGRAM

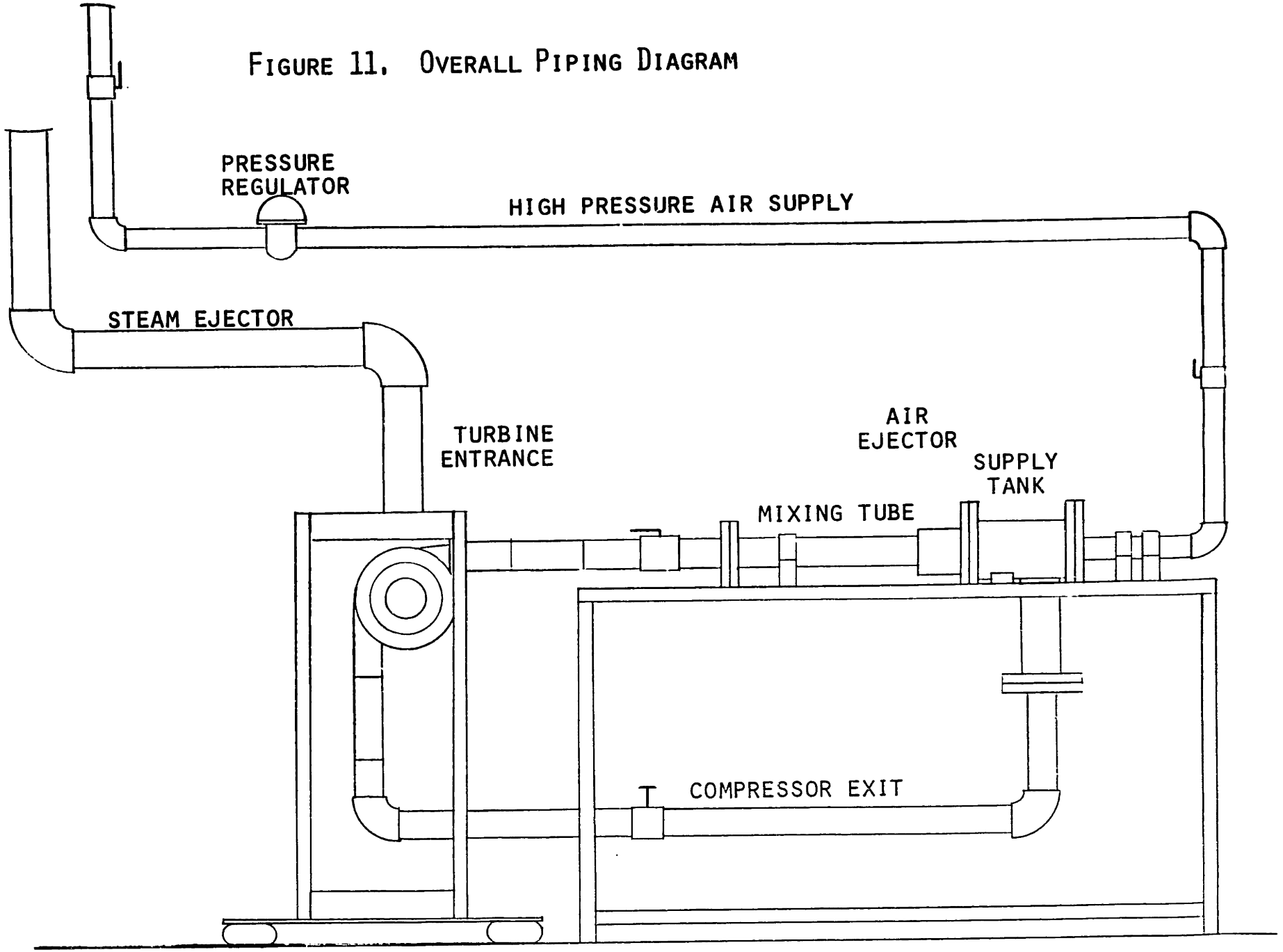

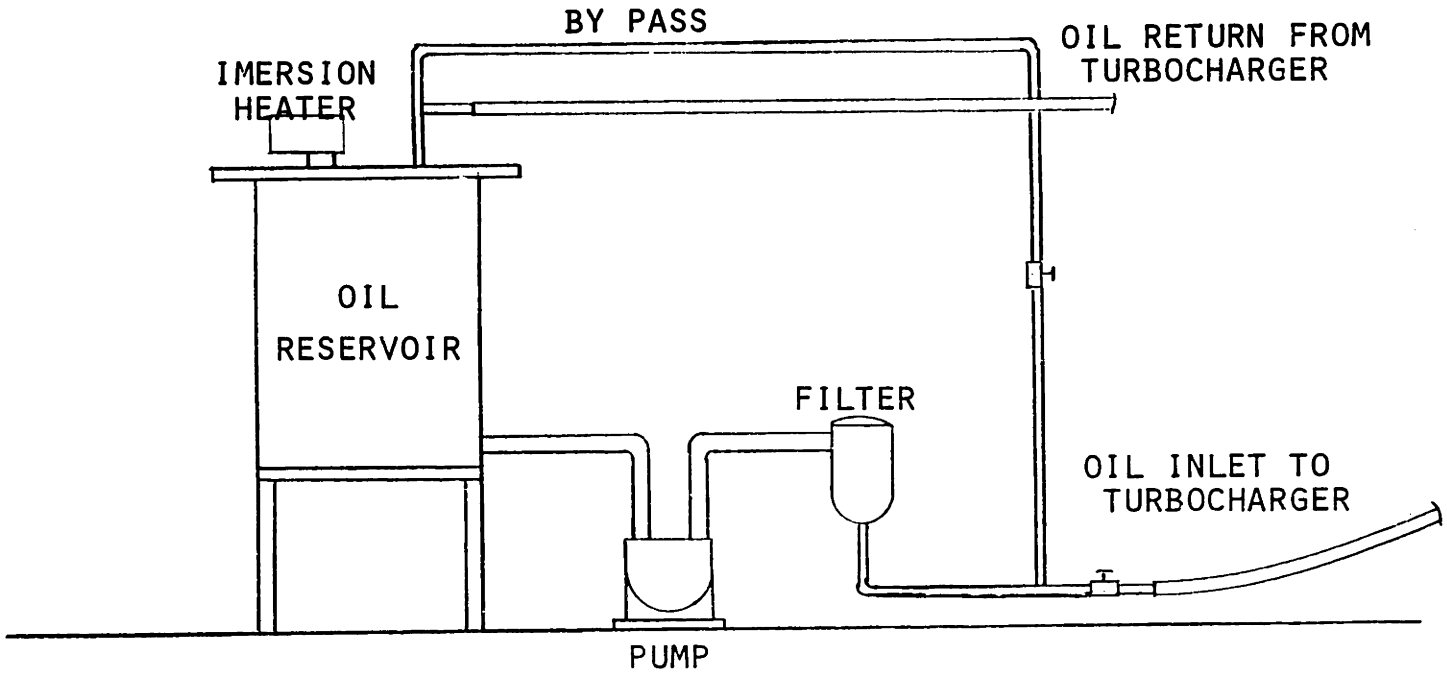

FIGURE 12. OIL PIPING DIAGRAM

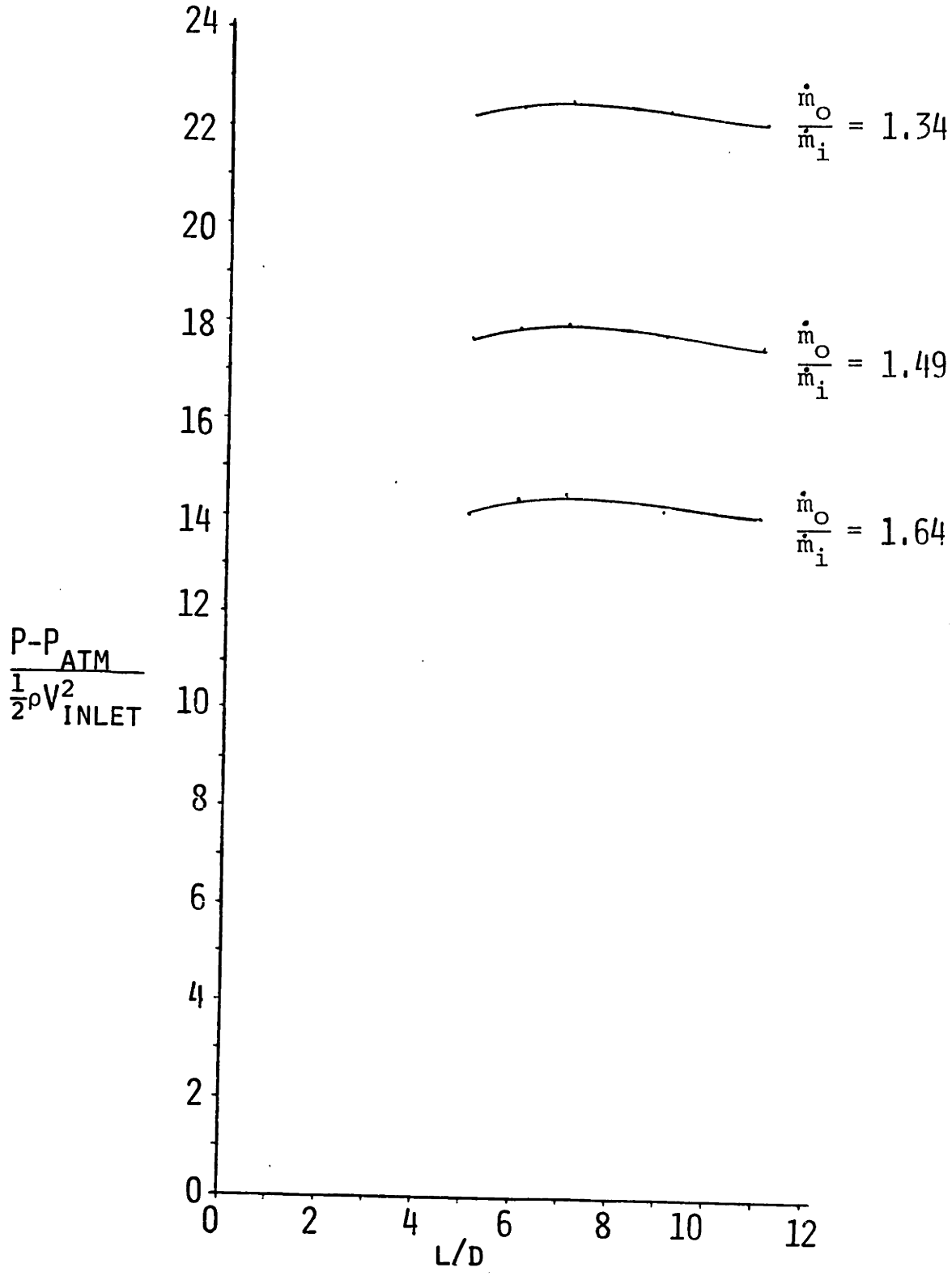

FIGURE 13. EXPERIMENTAL RESULTS FOR DETERMINATION OF MIXING TUBE LENGTH

FIGURE 14. VELOCITY PROFILES IN THE MIXING TUBE

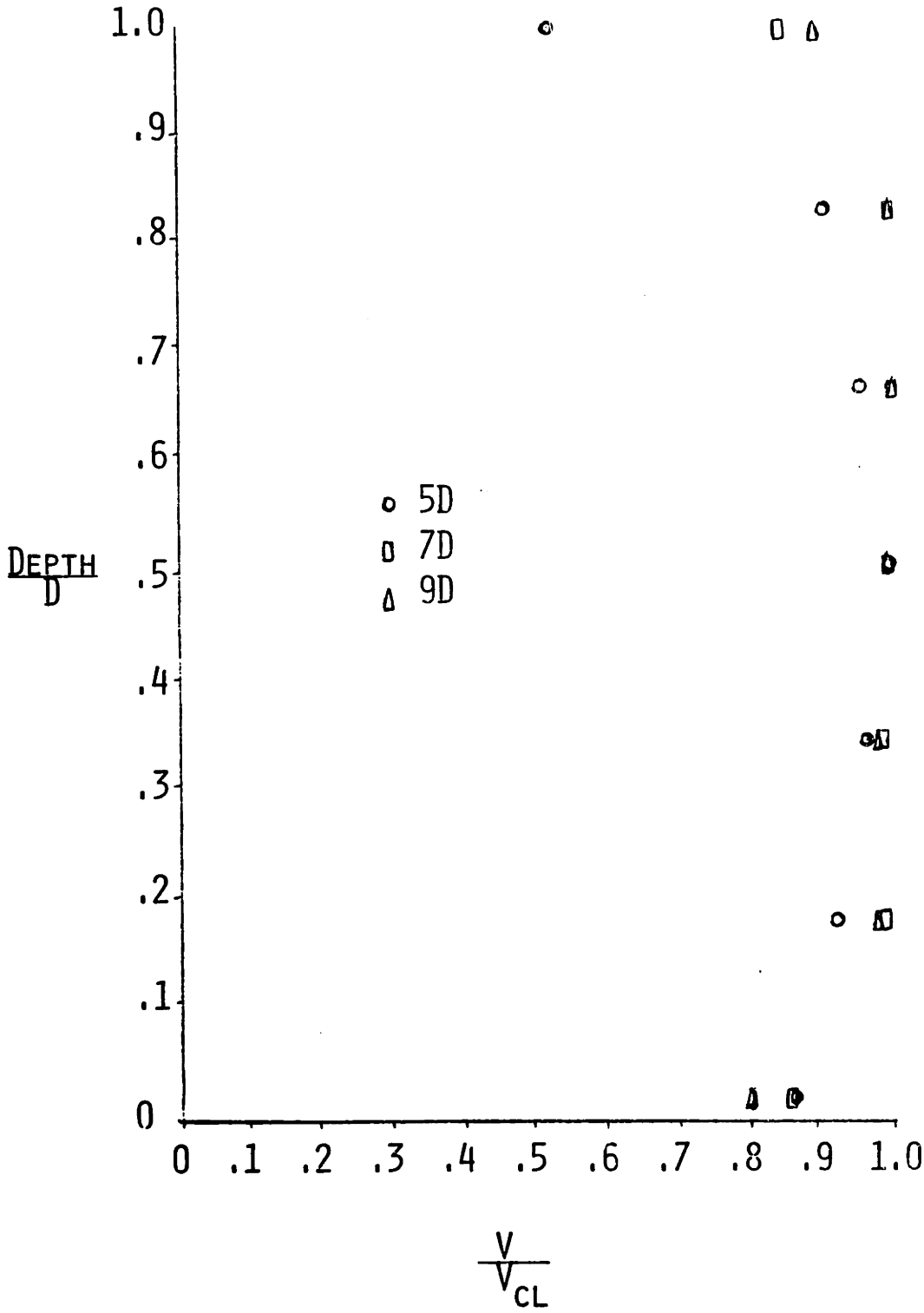

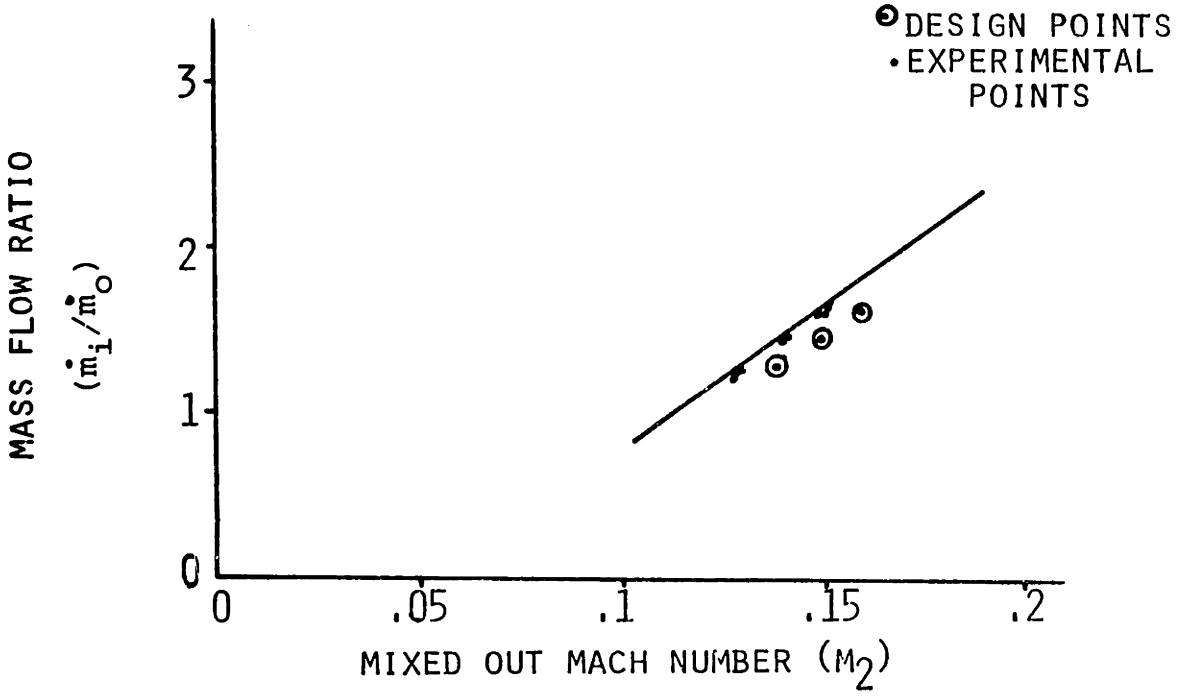

FIGURE 15. COMPARISON OF DESIGN AND MODELLING RESULTS TO EXPERIMENTAL MEASUREMENTS FOR $\dot{m}_i/\dot{m}_o$ VS M_2

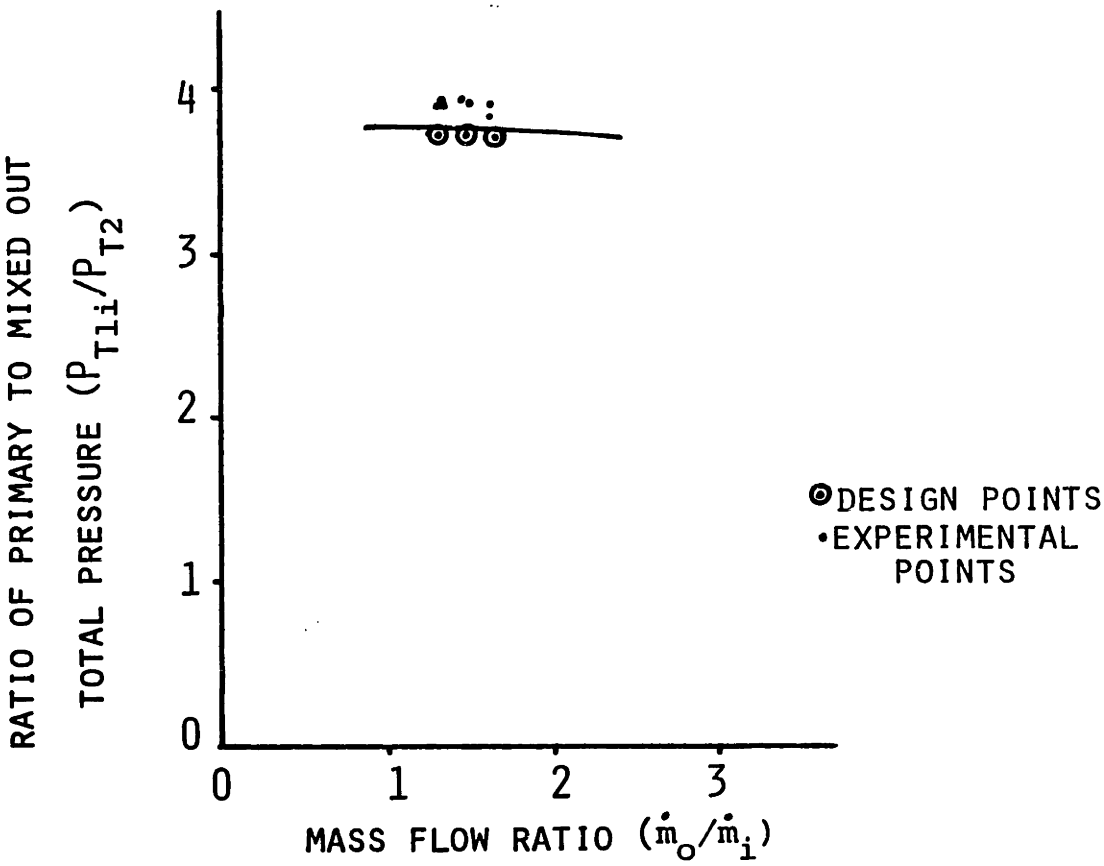

FIGURE 16. COMPARISON OF DESIGN AND MODELLING RESULTS TO EXPERIMENTAL MEASUREMENTS FOR P_{T_i}/P_{T2} VS $\dot{m}_o/\dot{m}_i$

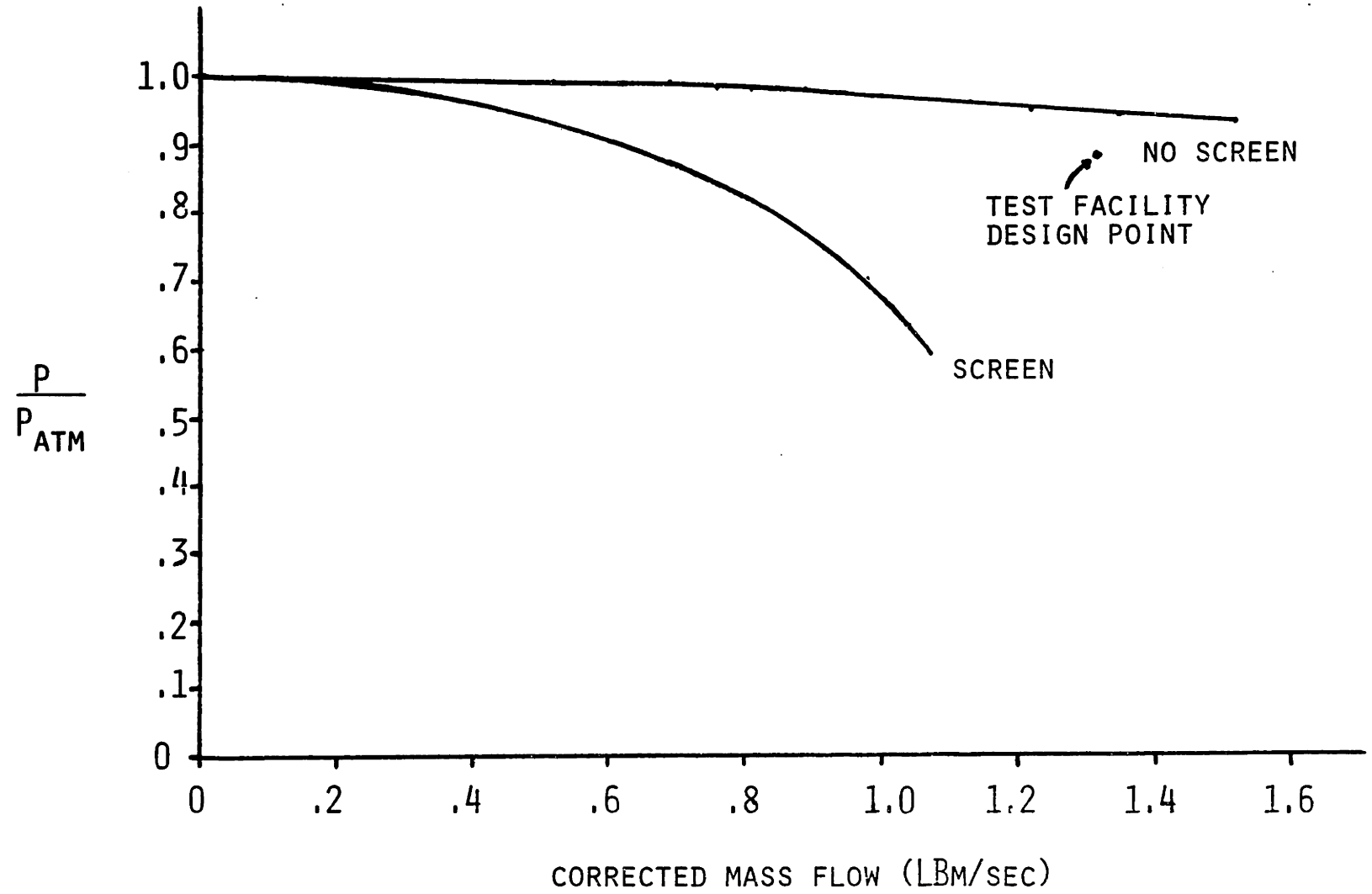

FIGURE 17. RESULTS OF STEAM EJECTOR TESTS (MASS FLOW RATE CORRECTED TO 14.696 PSI AND 545°R)

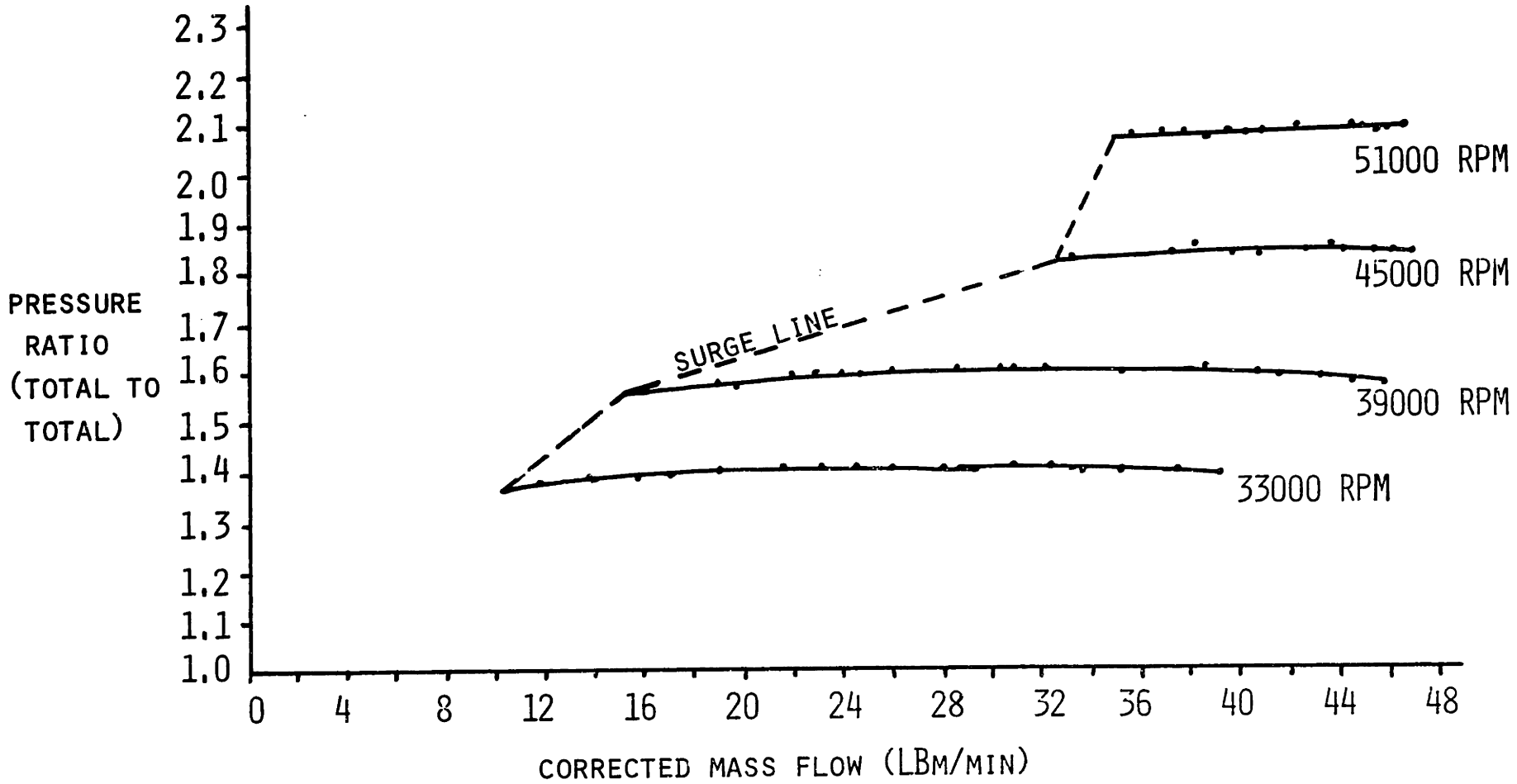

FIGURE 18. OVERALL COMPRESSOR CHARACTERISTIC (CORRECTED MASS FLOW VS TOTAL PRESSURE RATIO)

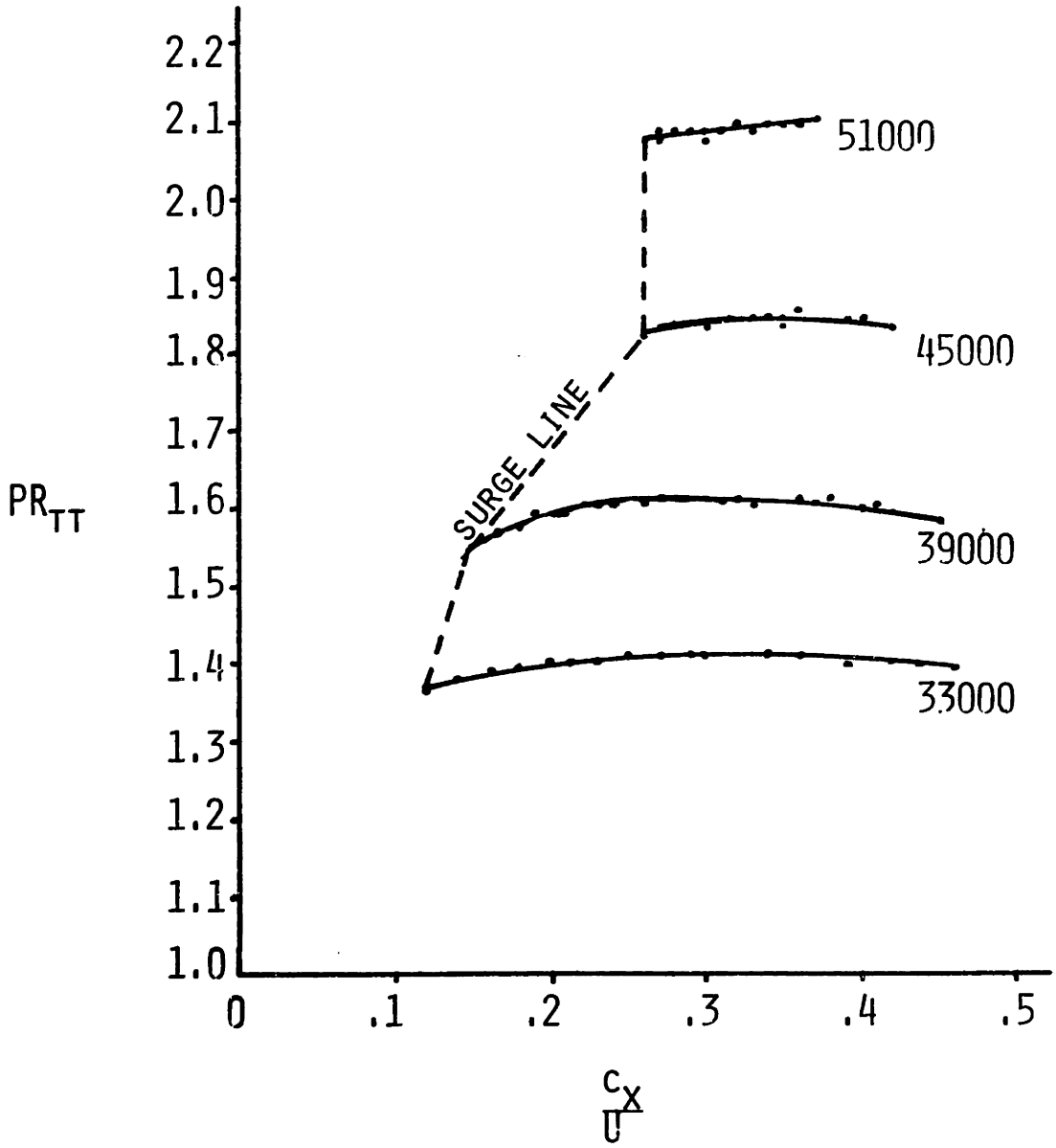

FIGURE 19. OVERALL COMPRESSOR CHARACTERISTIC

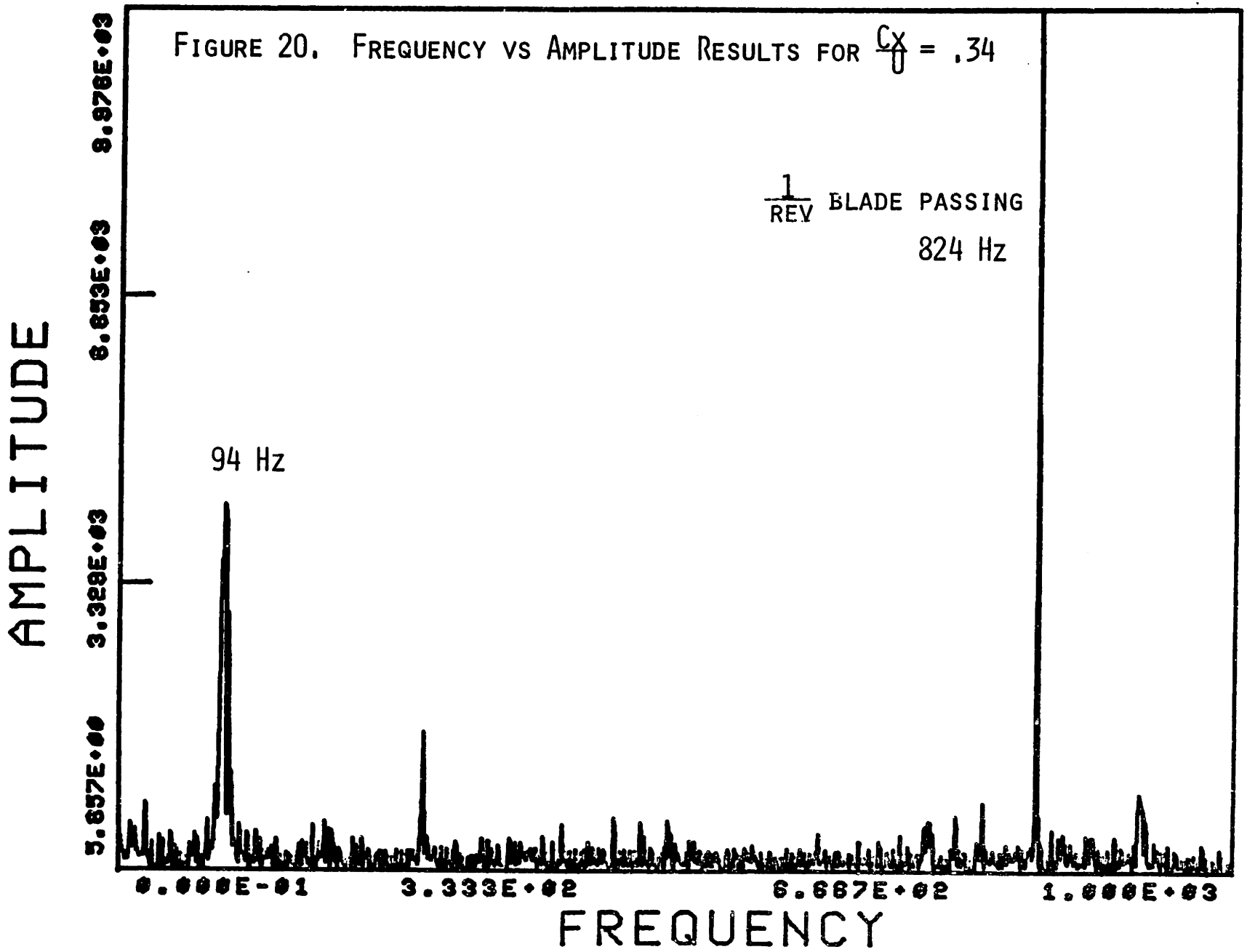
FIGURE 20. FREQUENCY VS AMPLITUDE RESULTS FOR $\frac{C_X}{0}$ = .34
$\frac{1}{REV}$ BLADE PASSING
824 Hz
94 Hz
AMPLITUDE
5.857E+00
3.329E+03
6.853E+03
9.876E+03
0.000E-01
3.333E+02
6.667E+02
1.000E+03
FREQUENCY

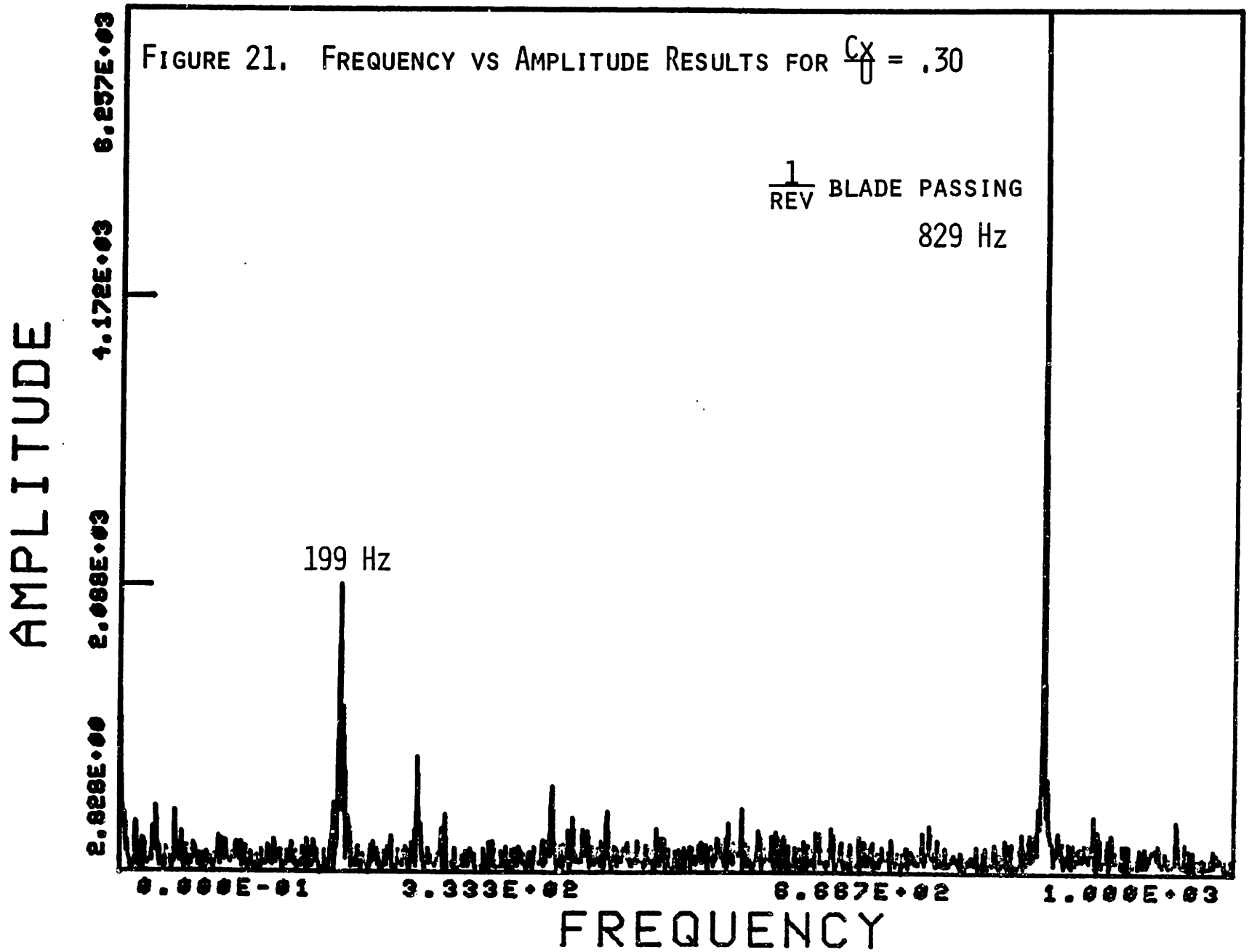
FIGURE 21. FREQUENCY VS AMPLITUDE RESULTS FOR $\frac{C_X}{0}$ = .30
$\frac{1}{REV}$ BLADE PASSING
829 Hz
199 Hz
AMPLITUDE
2.828E+00
2.088E+03
4.172E+03
6.257E+03
0.000E-01
3.333E+02
6.667E+02
1.000E+03
FREQUENCY

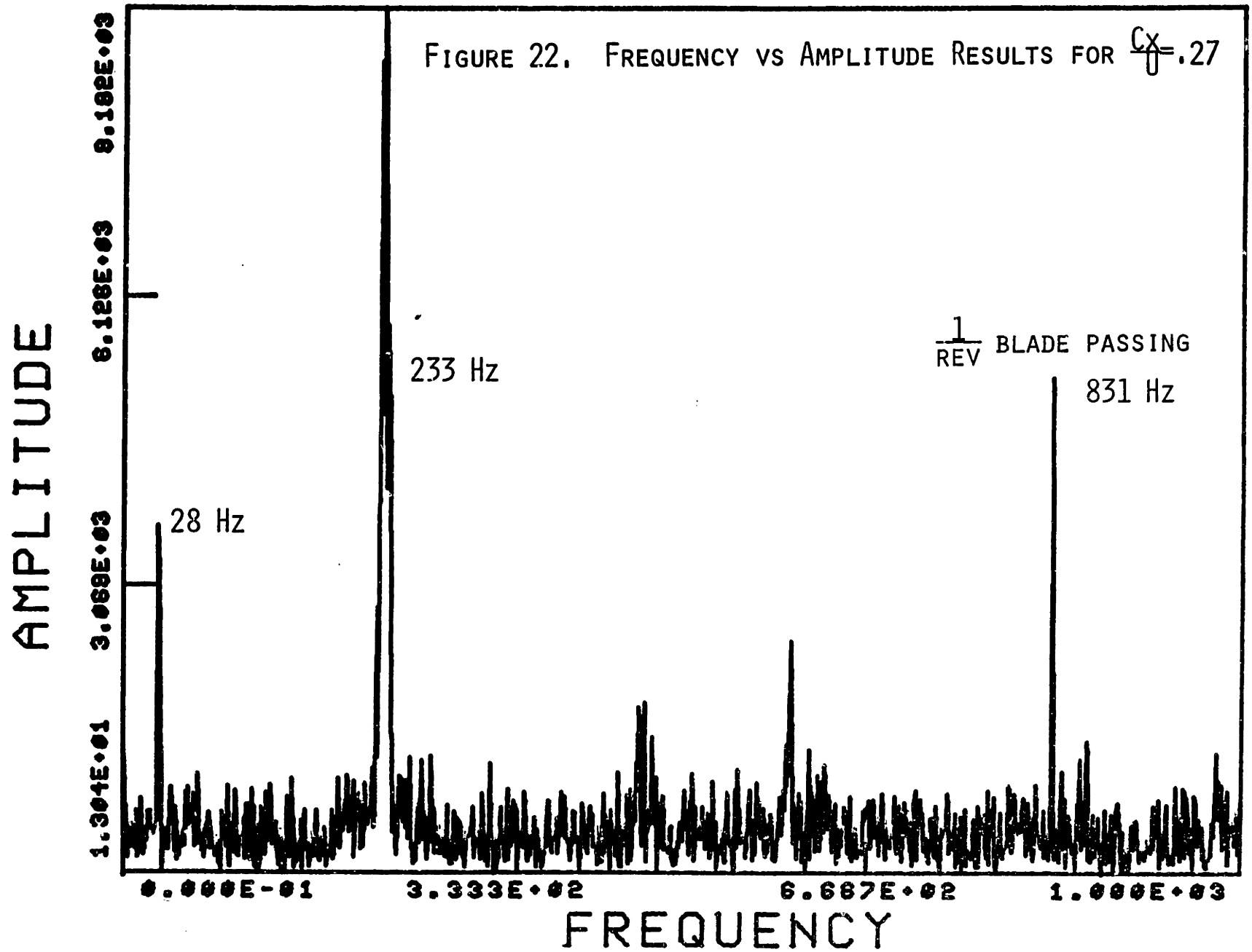

FIGURE 22. FREQUENCY VS AMPLITUDE RESULTS FOR $\frac{C_X}{\sigma}$=.27

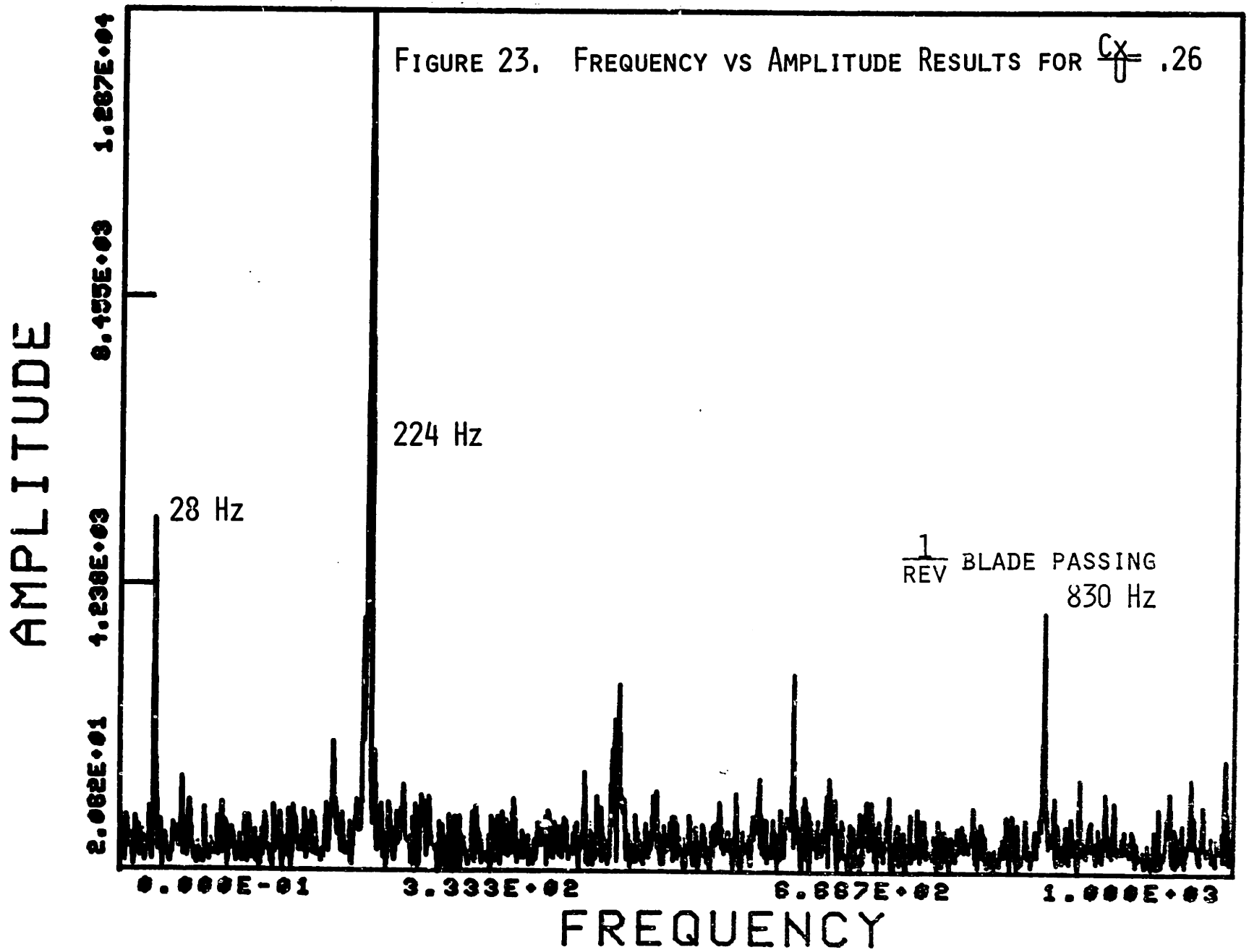

FIGURE 23. FREQUENCY VS AMPLITUDE RESULTS FOR $\frac{C_X}{0}$ = .26

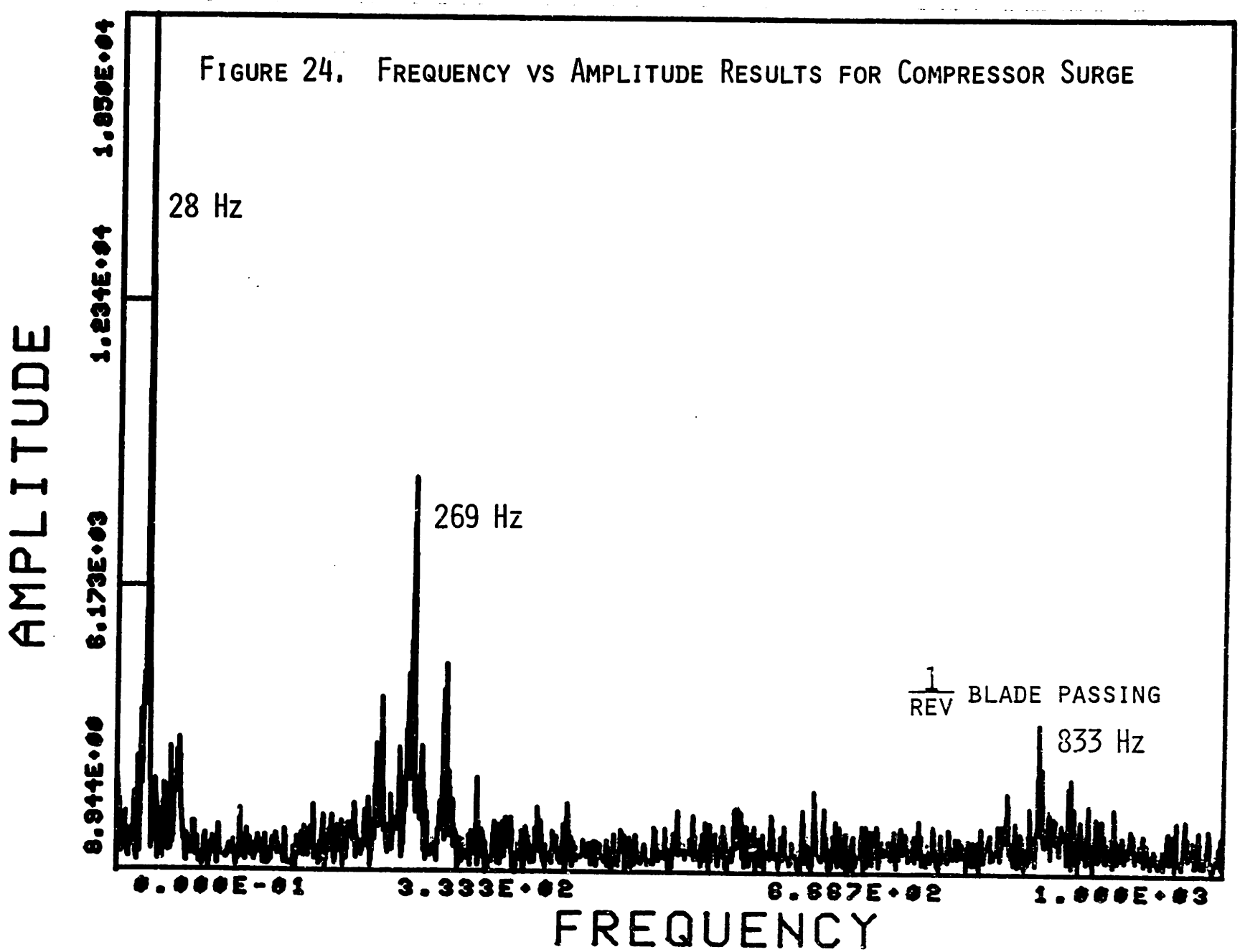

FIGURE 24. FREQUENCY VS AMPLITUDE RESULTS FOR COMPRESSOR SURGE

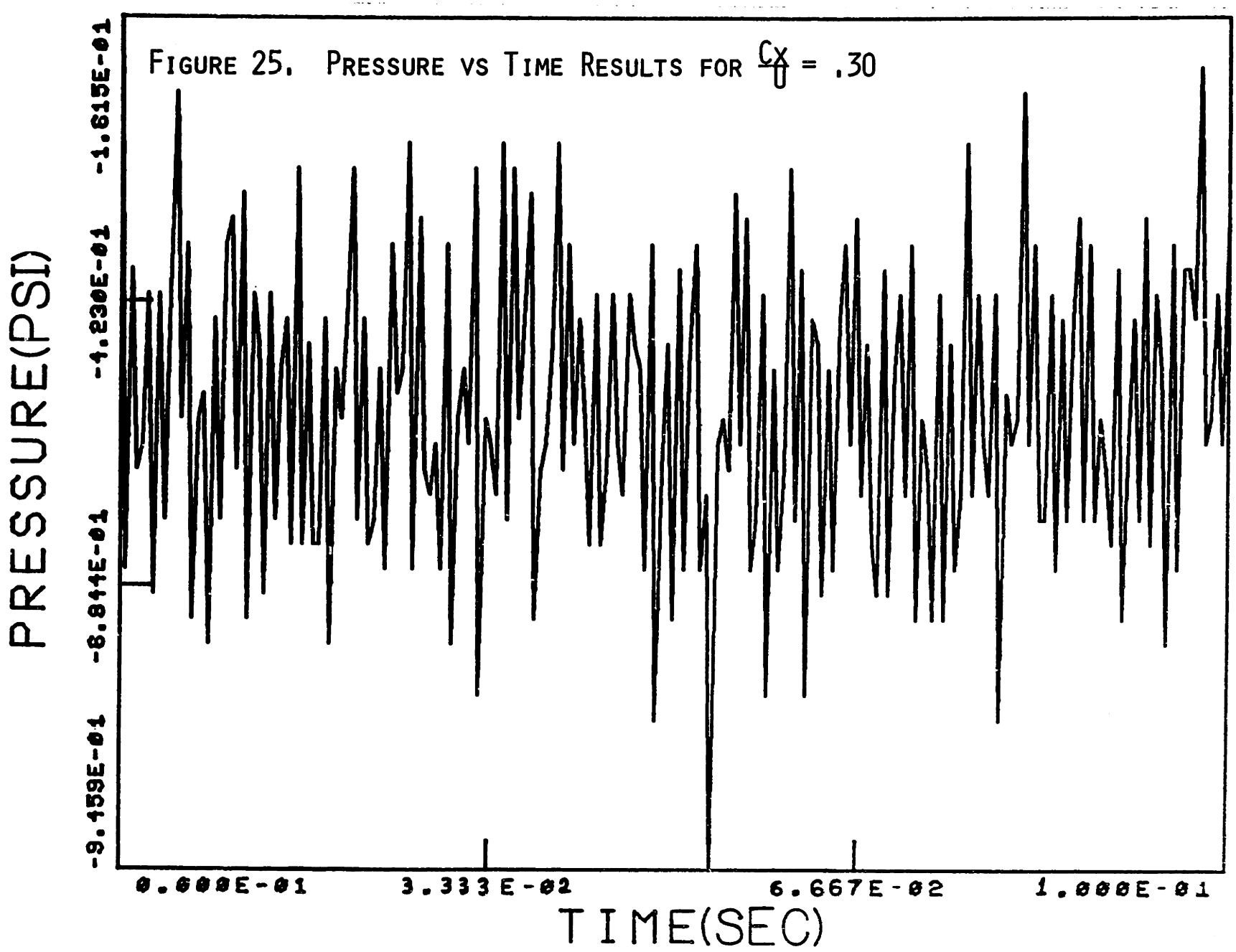
FIGURE 25. PRESSURE VS TIME RESULTS FOR $\frac{C_X}{0}$ = .30
PRESSURE(PSI)
-1.615E-01
-1.230E-01
-8.844E-01
-9.459E-01
0.000E-01
3.333E-02
6.667E-02
1.000E-01
TIME(SEC)

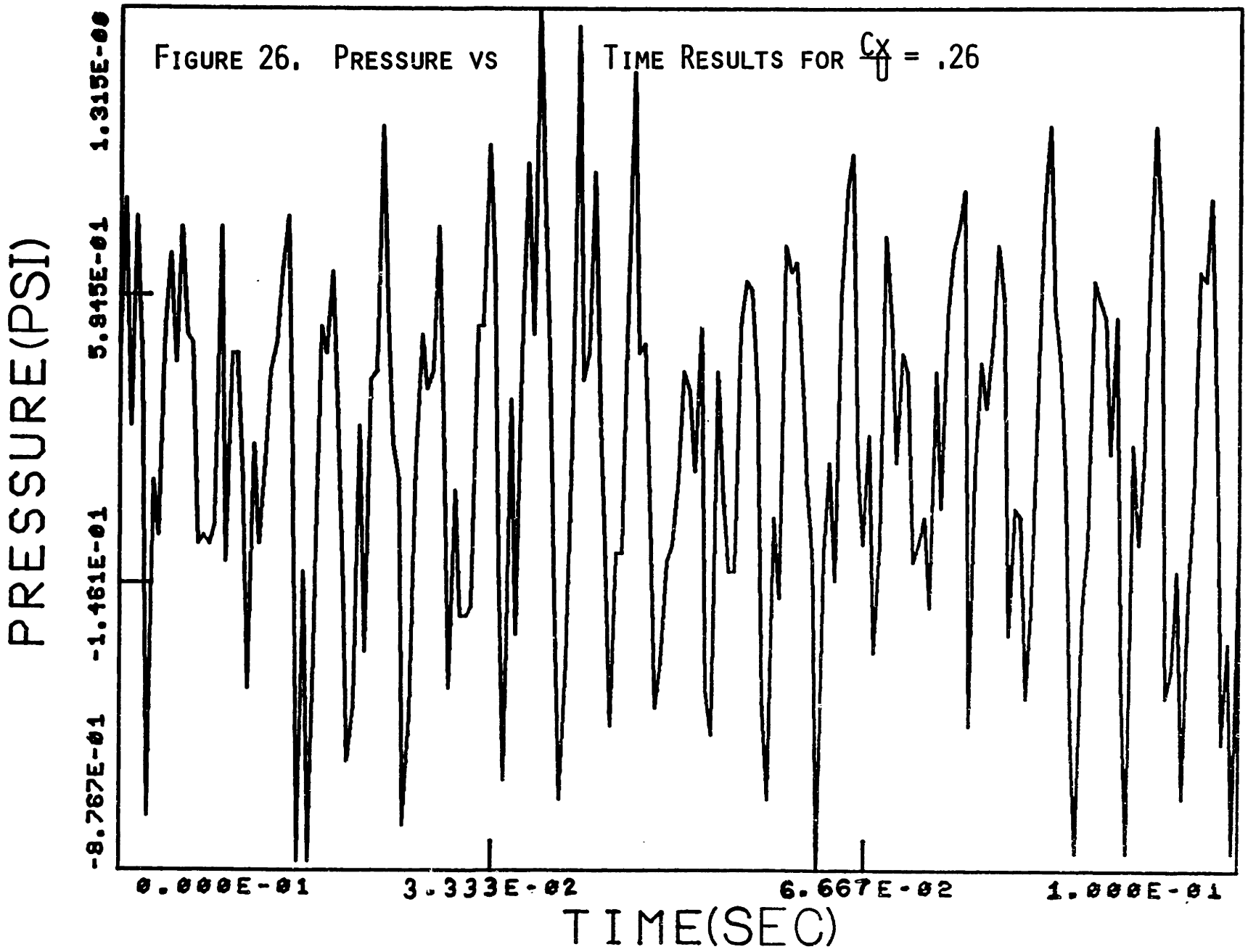
FIGURE 26. PRESSURE VS TIME RESULTS FOR $\frac{C_X}{0} = .26$
PRESSURE(PSI)
1.315E-00
5.845E-01
-1.461E-01
-8.767E-01
0.000E-01
3.333E-02
6.667E-02
1.000E-01
TIME(SEC)

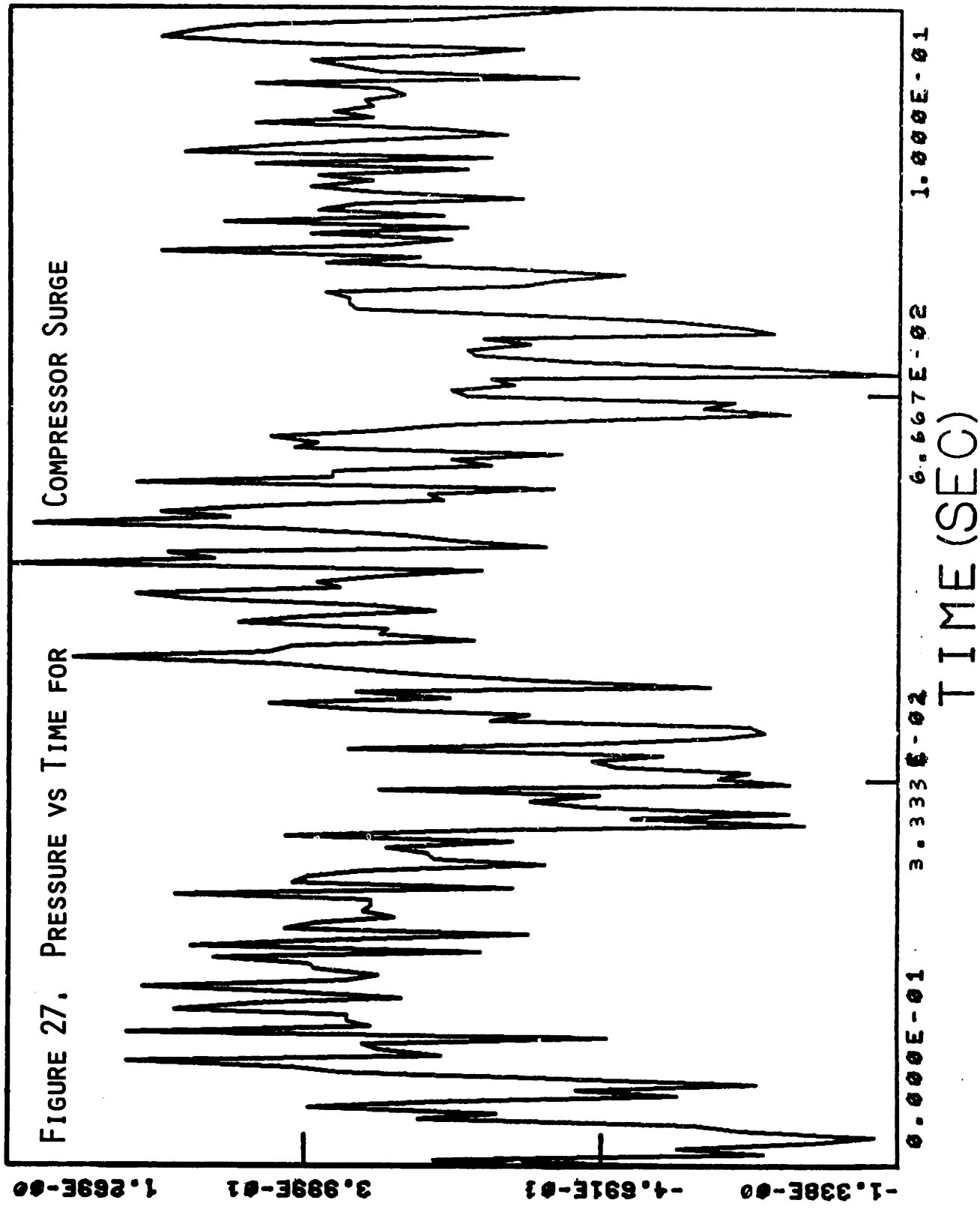
FIGURE 27. PRESSURE VS TIME FOR COMPRESSOR SURGE
PRESSURE (PSI)
1.2696E-00
3.9998E-01
-4.691E-01
-1.338E-00
0.0000E-01
3.333E-02
6.667E-02
1.000E-01
TIME (SEC)

APPENDIX A

In this section the design of an axial symmetric convergent-divergent nozzle will be described.

To determine the geometry of the divergent portion of a nozzle for uniform parallel flow at nozzle exit the analytical technique presented by Foelsch [11] was used. The required parameters for this analysis are the nozzle exit Mach number and diameter. It is assumed that the fluid behaves like a perfect gas with constant specific heats.

The first step in this analysis is to determine the constants ϕ_E and τ_E at the nozzle exit (see Figure A-1 for the nomenclature). These quantities are found using the following equations, with M being the nozzle exit Mach number.

$$\phi = \frac{1}{2}\left[\sqrt{\frac{\gamma+1}{\gamma-1}}\tan^{-1}\sqrt{\frac{\gamma-1}{\gamma+1}(M^2-1)} - \tan^{-1}\sqrt{M^2-1}\right] \qquad A.1$$

$$\tau^2 = \frac{\left(\frac{2}{\gamma+1} + \frac{\gamma-1}{\gamma+1}M^2\right)^{\frac{\gamma+1}{2(\gamma-1)}}}{M} \qquad A.2$$

In the second step, ϕ_E is used to determine the constant ω

$$\omega = (1/2)\ \phi_E \qquad A.3$$

but ω is also equal to θ_A amd ϕ_A;

$$\omega = (1/2)\ \phi_E = \Theta_A = \phi_A \qquad \text{A.4}$$

Next τ_A and $\sqrt{M_A^2-1}$ are found for $\phi_A = (1/2)\ \phi_E$ through use of Table 1 in reference [11].

In step three the x and y coordinates of the section AB are found by varying $\sqrt{M^2-1}$ from $\sqrt{M_A^2-1}$ to $\sqrt{M_{i1}^2-1}$. For the $\sqrt{M^2-1}$ chosen between A and B the following equations are used:

$$\phi = \frac{1}{2}\left[\sqrt{\frac{\gamma+1}{\gamma-1}}\ \tan^{-1}\sqrt{\frac{\gamma-1}{\gamma+1}\ (M^2 - 1)} - \tan^{-1}\sqrt{M^2 - 1}\right] \qquad \text{A.1}$$

$$\Theta = \phi_E - \phi \qquad \text{A.5}$$

$$\tau^2 = \frac{\left(\frac{2}{\gamma+1} + \frac{\gamma-1}{\gamma+1}\ M^2\right)^{\frac{\gamma+1}{2(\gamma-1)}}}{M} \qquad \text{A.2}$$

$$F(\Theta) = \sqrt{\sin^2\Theta + 2(\cos\Theta - \cos\ \omega)(\sqrt{M^2-1}\ \sin\Theta + \cos\Theta)} \qquad \text{A.6}$$

$$y = (D_E/4)\ \sin\ (\omega/2)\ (\tau/\tau_E)\ F(\Theta) \qquad \text{A.7}$$

$$x = \frac{D_E}{4}\ \sin\ (\omega/2)\ \frac{\tau}{\tau_E}\ \frac{1 + (\cos\Theta\ \sqrt{M^2-1} - \sin\Theta)F(\Theta)}{\sin\Theta\ \sqrt{M^2-1} + \cos\Theta}$$

where D_E is the nozzle exit diameter.

In step four x_o is determined from equation A.8 and subtracted from all the x's obtained in step three.

$$x_o = \frac{D_E}{2\tau_E}\left[\cot\omega - \frac{\tau_A\ \cos(\omega/2) - 1}{2\cos(\omega/2)[\sin(\omega/2) + \cos(\omega/2)]}\right] \qquad \text{A.8}$$

The final step consists of calculating λ and R from equation A.9 and determining the coordinates of point D by using equation A.10.

$$R = \lambda = \frac{D_E}{4\tau} \frac{\tau_A \cos(\omega/2) - 1}{\sin(\omega/2)\ \cos(\omega/2) + \sin(\omega/2)} \qquad A.9$$

$$x_D = R \sin\omega \qquad y_D = \frac{D_E}{2\tau_E} + R(1-\cos\omega) \qquad A.10$$

The values of y calculated in equation A.7 are for a perfect fluid, so some boundary layer displacement thickness must be added to compensate for the mass flow in each cross section of the nozzle. From information found in reference [40] boundary layer correction can be applied to each of the above calculated coordinates. In this work a correlation was presented for Mach number versus $[(\delta^* Re^{1/5})/(x^{4/5})]$. Thus for each $\sqrt{M^2-1}$ between $\sqrt{M_A^2-1}$ and $\sqrt{M_{i1}^2-1}$, $[(\delta^* Re^{1/5})/(x^{4/5})]$ was obtained from Figure 23 in reference [40] and the displacement thickness added to the y coordinate calculated in equation A.7.

The convergent portion of the nozzle can be designed in accordance with the method presented by Morel [24]. In this method the information necessary to design a nozzle contraction is specified by the values of Cp_{inlet} and Cp_{exit}, the maximum wall pressure coefficients, for contraction ratios greater than 4 (the contraction ratio being defined as the nozzle inlet area divided by the throat area). The throat area is calculated as part of the divergent nozzle design.

The values of Cp_{inlet} and Cp_{exit} were chosen to be .35 and .04 to avoid boundary layer separation at inlet and exit [24]. Knowing these values and the contraction ratio (must be above 4), the design of a nozzle contraction is relatively simple. The first step is to determine the values of the variables F_e and G_i for the contraction ratio; F_e is found from Figure 10 of reference [24] for Cp_{exit} = .04, and G_i is found from Figure 11 [24] for Cp_{inlet} = .35.

The values of F_e and G_i are then used to determine the value of X. The parameter X is used as the sole representative of the wall contour by Morel [24]. The wall contour is constructed from two matching cubics (see Figure A-2) with $X = x_m/L_c$. X was determined from equation A.11 and Figure 12 of reference [24].

$$\frac{X^{1/2}}{(1-X)^{2/3}} = F_e^{1/3}\, G_i^{-1/2}\, m^{1/2}(m-1)^{1/6} \qquad \text{A.11}$$

where $$m = \frac{D_{inlet}}{D_{throat}}$$

With the value of X established the convergent length and coordinates of the wall contour can be calculated. The length of the convergent portion of the nozzle is calculated from equation A.12.

$$\frac{L_c}{D_{inlet}} = \left(\frac{m}{(m-1)}\, G_i\, X\right)^{-1/2} \qquad \text{A.12}$$

(This design procedure gives the shortest contraction length possible.) The wall contour coordinates are calculated using equation A.13.

$$\frac{D}{D_{inlet}} = 1 - \frac{m-1}{m}\,\frac{1}{X^2}\left(\frac{x}{L_c}\right)^3 \quad \text{for } \frac{x}{L_c} \leq X$$

$$\frac{D}{D_{throat}} = 1 + \frac{m-1}{(1-X)^2}\left(1 - \frac{x}{L_c}\right)^3 \quad \text{for } \frac{x}{L_c} > X \qquad \text{A.13}$$

Thus x/L_c was varied from 0 to 1 and the wall contour determined.

Using this method, the convergent-divergent nozzle required by the ejection system was designed. The tolerances were chosen which gave the least variation of nozzle exit Mach number.

Table A-1. Convergent-Divergent Nozzle Coordinates

X (in)	I.D. (in)	O.D. (in)	X (in)	I.D. (in)	O.D. (in)	
5.25	2.000±0.003	2.600±0.005	2.00	0.899±0.003	1.199±0.005	
5.20	2.000±0.003	2.600±0.005	1.90	0.839±0.003	1.139±0.005	
5.10	2.000±0.003	2.598±0.005	1.80	0.784±0.003	1.084±0.005	
5.00	2.000±0.003	2.595±0.005	1.70	0.735±0.003	1.035±0.005	
4.90	1.999±0.003	2.593±0.005	1.60	0.691±0.003	0.991±0.005	
4.80	1.998±0.003	2.490±0.005	1.50	0.652±0.003	0.952±0.005	
4.70	1.996±0.003	2.587±0.005	1.40	0.619±0.003	0.919±0.005	
4.60	1.993±0.003	2.585±0.005	1.30	0.590±0.003	0.890±0.005	
4.50	1.989±0.003	2.577±0.005	1.20	0.564±0.003	0.864±0.005	
4.40	1.984±0.003	2.566±0.005	1.10	0.543±0.003	0.843±0.005	
4.30	1.984±0.003	2.552±0.005	1.00	0.525±0.003	0.825±0.005	
4.20	1.967±0.003	2.535±0.005	0.90	0.511±0.003	0.811±0.005	
4.10	1.955±0.003	2.514±0.005	0.80	0.499±0.003	0.799±0.005	
4.00	1.941±0.003	2.488±0.005	0.70	0.490±0.003	0.790±0.005	
3.90	1.925±0.003	2.456±0.005	0.60	0.483±0.003	0.783±0.005	
3.80	1.905±0.003	2.421±0.005	0.50	0.478±0.003	0.778±0.005	
3.70	1.883±0.003	2.381±0.005	0.40	0.475±0.003	0.775±0.005	
3.60	1.857±0.003	2.332±0.005	0.30	0.473±0.003	0.773±0.005	
3.50	1.828±0.003	2.271±0.005	0.20	0.472±0.003	0.772±0.005	
3.40	1.795±0.003	2.194±0.005	0.10	0.472±0.003	0.772±0.005	
3.30	1.758±0.003	2.129±0.005	0.00	0.472±0.001	0.772±0.005	REF
3.20	1.717±0.003	2.058±0.005	0.05	0.478±0.003	0.776±0.005	
3.10	1.671±0.003	1.987±0.005	0.10	0.486±0.003	0.763±0.005	
3.00	1.621±0.003	1.921±0.005	0.15	0.494±0.003	0.758±0.005	
2.90	1.566±0.003	1.866±0.005	0.20	0.500±0.003	0.754±0.005	
2.80	1.505±0.003	1.805±0.005	0.25	0.507±0.003	0.749±0.005	
2.70	1.440±0.003	1.740±0.005	0.30	0.512±0.003	0.744±0.005	
2.60	1.369±0.003	1.669±0.005	0.35	0.516±0.003	0.740±0.005	
2.50	1.292±0.003	1.592±0.005	0.40	0.520±0.003	0.735±0.005	
2.45	1.251±0.003	1.551±0.005	0.45	0.524±0.003	0.730±0.005	
2.40	1.209±0.003	1.509±0.005	0.50	0.527±0.003	0.726±0.005	
2.35	1.165±0.003	1.465±0.005	0.55	0.530±0.003	0.721±0.005	
2.30	1.122±0.003	1.422±0.005	0.60	0.532±0.003	0.717±0.005	
2.25	1.081±0.003	1.381±0.005	0.65	0.534±0.003	0.712±0.005	
2.20	1.041±0.003	1.341±0.005	0.70	0.536±0.003		
2.10	0.967±0.003	1.267±0.005	0.75	0.538±0.003		
			0.78	0.540±0.003		

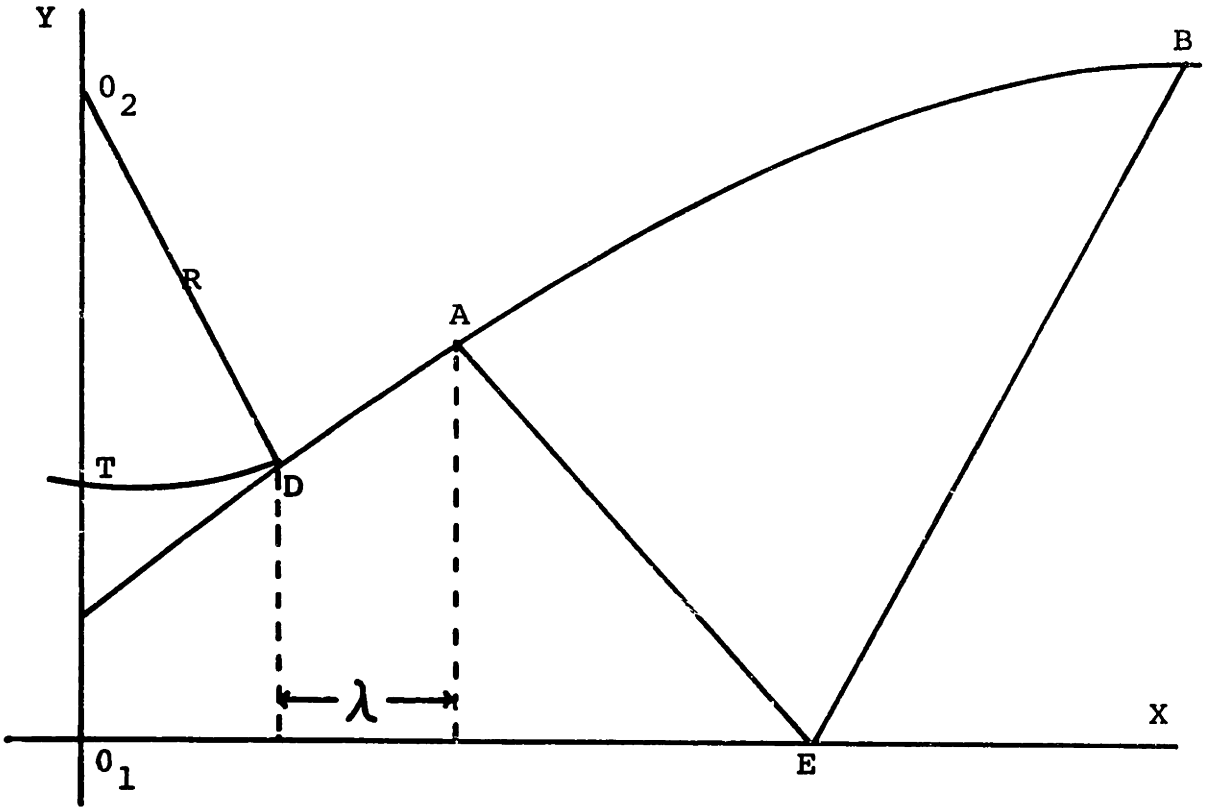

FIGURE A-1. NOMENCLATURE FOR DIVERGENT DESIGN

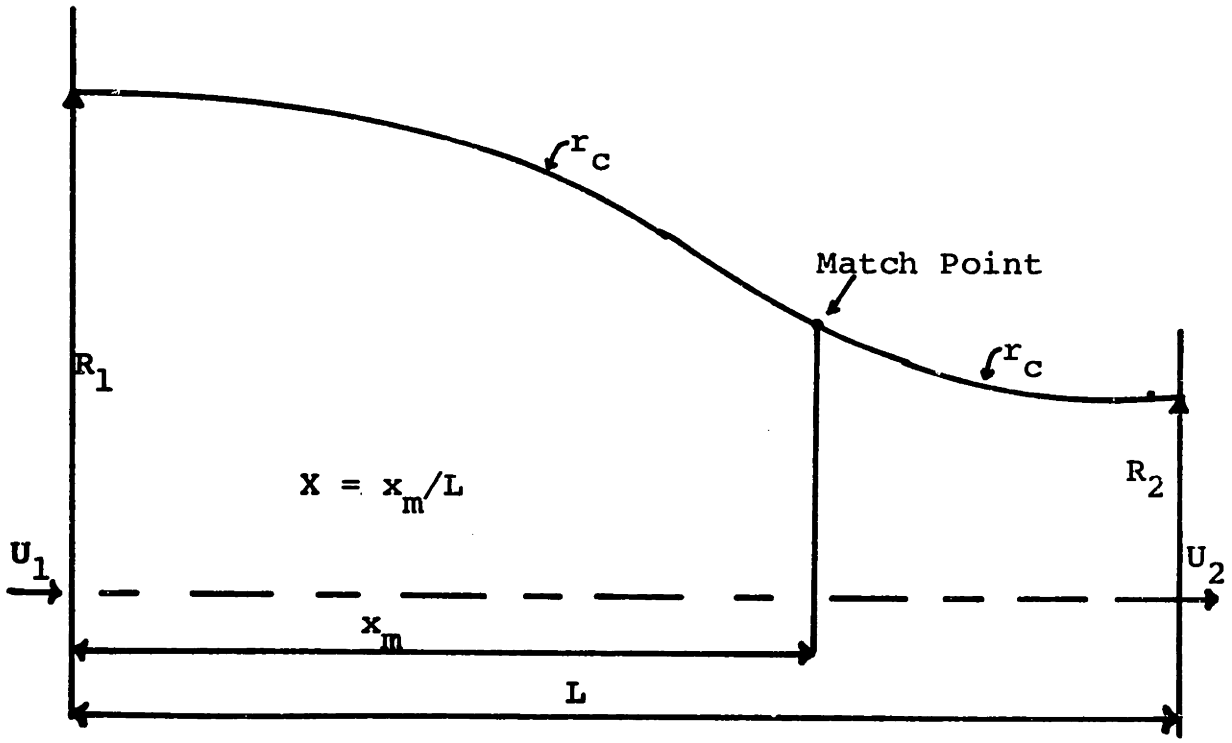

FIGURE A-2. NOMENCLATURE FOR CONVERGENT DESIGN

APPENDIX B

This section shows the supply tank and the end plate used in the design of the ejection system. In addition, the coordinates used for the converging mixing tube entrance are given.

Table B-1. Mixing Tube Entrance

X (in)	D (in)	X (in)	D (in)
0.0	6.065±0.005	2.6	3.456±0.005
0.2	6.051±0.005	2.8	3.361±0.005
0.4	5.951±0.005	3.0	3.283±0.005
0.6	5.679±0.005	3.2	3.221±0.005
0.8	5.327±0.005	3.4	3.172±0.005
1.0	5.009±0.005	3.6	3.134±0.005
1.2	4.722±0.005	3.8	3.107±0.005
1.4	4.465±0.005	4.0	3.089±0.005
1.6	4.236±0.005	4.2	3.077±0.005
1.8	4.033±0.005	4.4	3.071±0.005
2.0	3.855±0.005	4.6	3.069±0.005
2.2	3.701±0.005	4.8	3.068±0.005
2.4	3.568±0.005	4.85	3.068±0.005

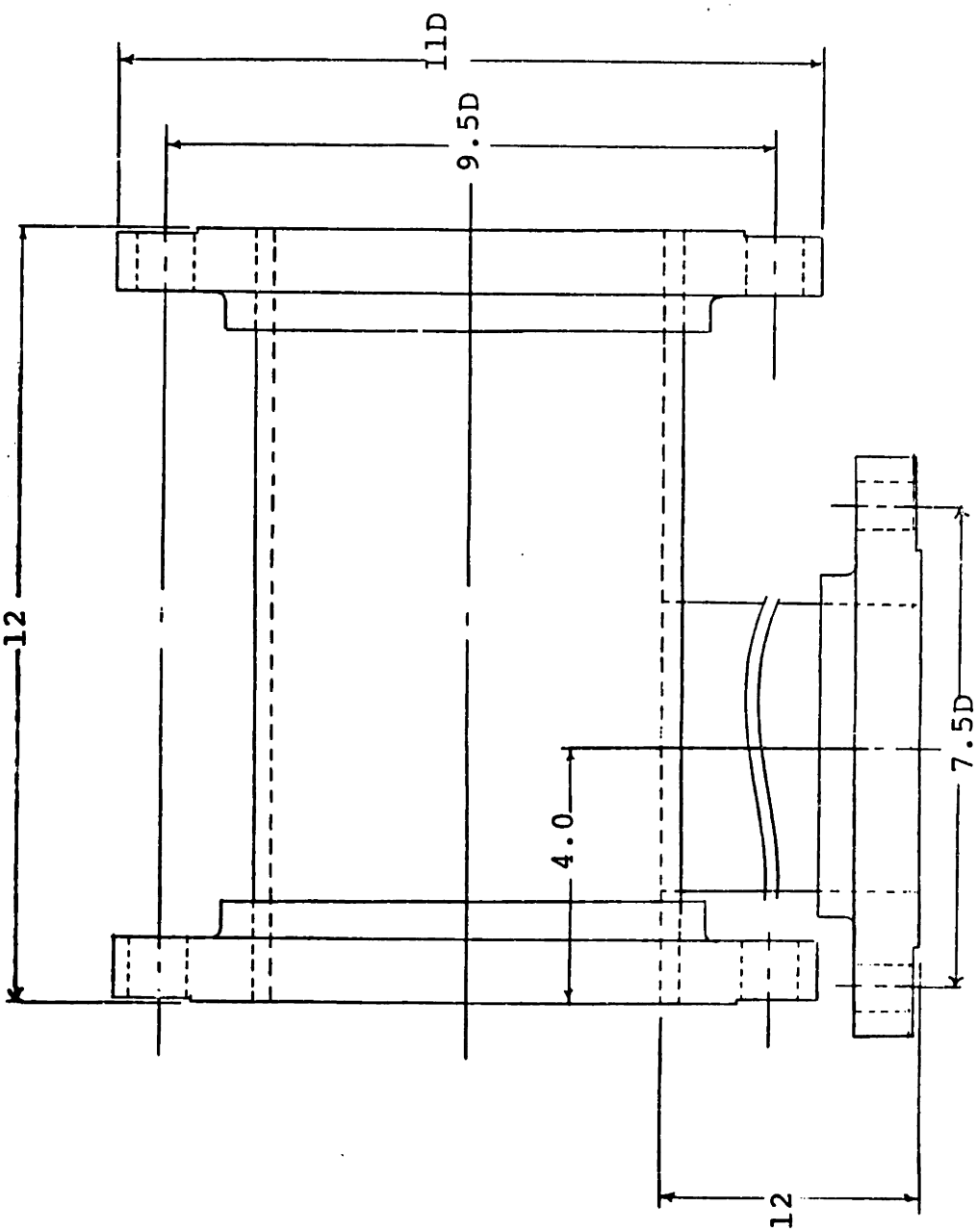

FIGURE B-1. SUPPLY TANK (ALL DIMENSIONS IN INCHES)

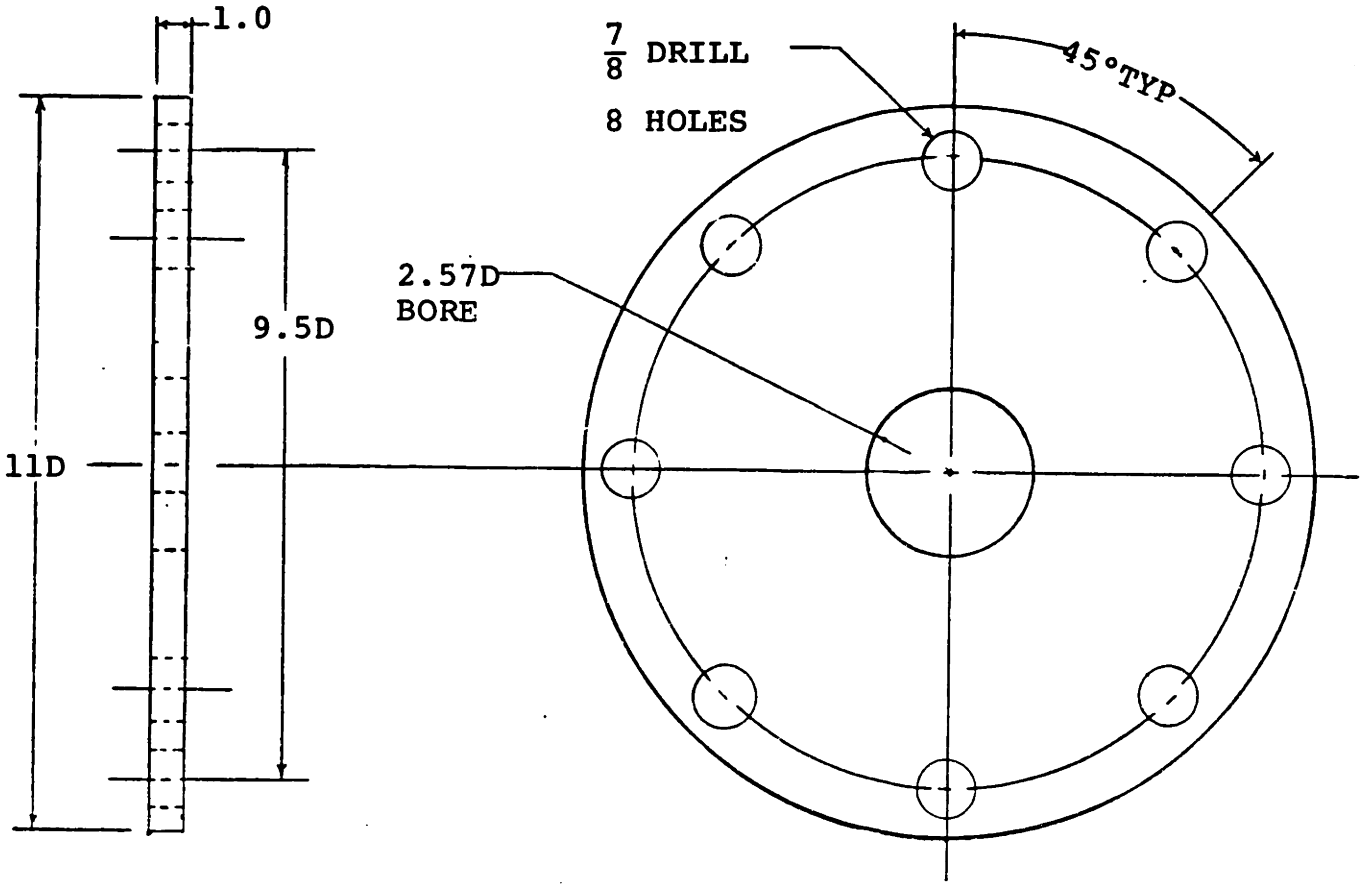

FIGURE B-2. SUPPLY TANK END PLATE

(ALL DIMENSIONS IN INCHES)

APPENDIX C

In this section the computer programs are presented which were used to obtain the overall compressor characteristic and the dynamic response of the compressor. Also, shown is a schematic diagram of the data acquisition system (Figure C-1). In addition, the programs are shown which were used to perform the Fast Fourier Transform on the data and plot the results as frequency versus amplitude.

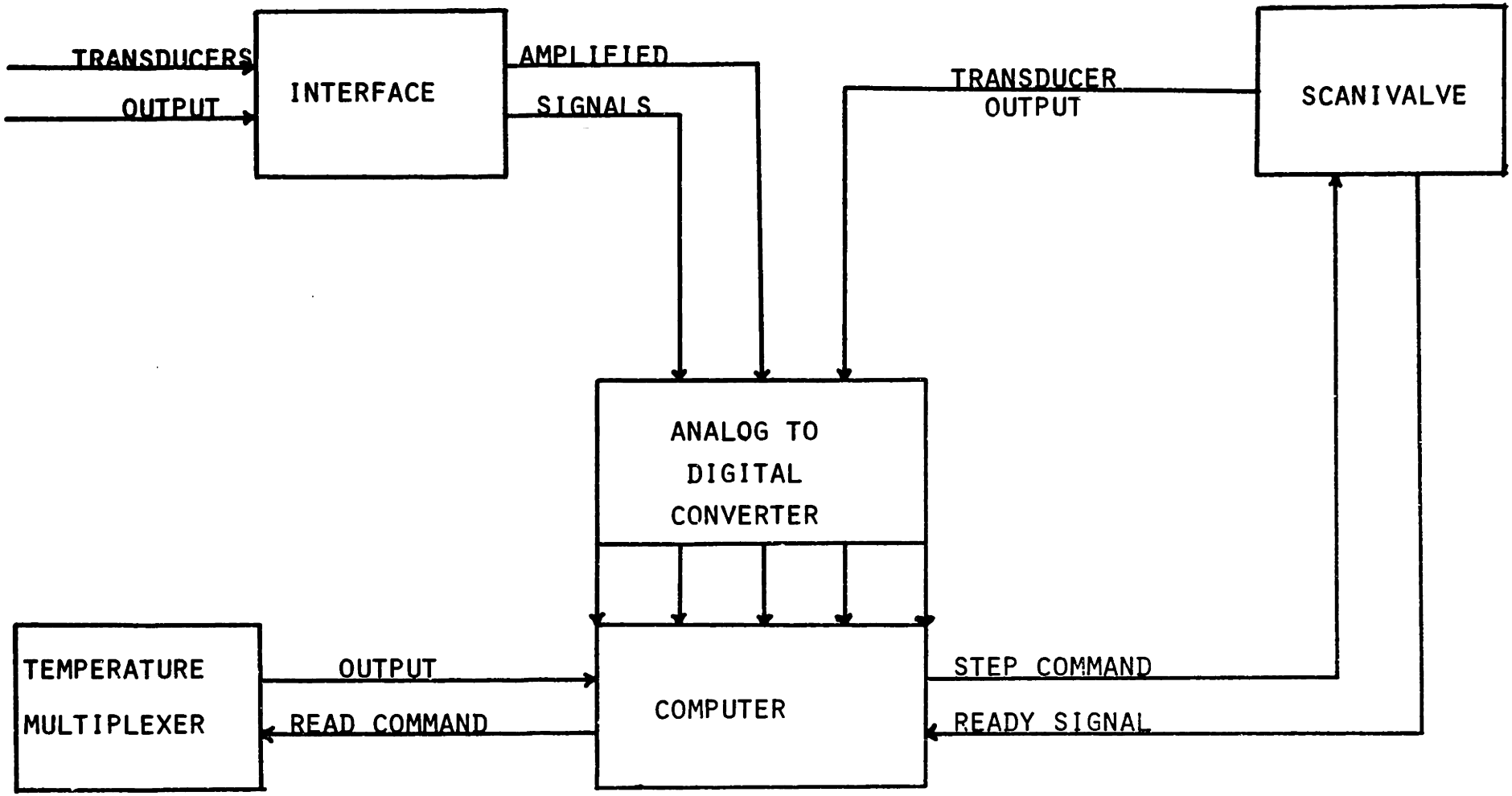

FIGURE C-1. SCHEMATIC DIAGRAM OF DATA ACQUISITION SYSTEM

STEADY AND UNSTEADY DATA ACQUISITION PROGRAM

```
C THIS PROGRAM CONTROLS THE ACQUISION OF STEADY AS WELL AS
C UNSTEADY DATA. THE SCANI VALVE SHOULD BE ON CHANNEL 0 OF
C THE A/D CONVERTER.THE DYNAMIC RESPONSE PROBES SHOULD BE
C ON CHANNELS 1 AND 2.
C     ASSIGN LINE PRINTER 6:ASSIGN LP 6
C     ASSIGN THE FLOPPY DISK 8:ASSIGN DY1: 8
          DIMENSION P(48),ID(30),T(7),XA(100),YA(100),IBUF(30)
          DIMENSION ID1(2048),ID2(2048)
          BYTE SPEED1(17),SPEED2(17),HPROB(13)
          DATA HPROB/'D','Y','1',':','U','S',' ',' ',
     1'.','D','A','T',0/
          KL=5
          INCR=0
          WRITE(5,*)'ENTER THE DATE:MONTH,DAY,YEAR'
          ACCEPT*,IMONTH,IDAY,IYEAR
          WRITE(5,*)'ENTER PAMB AND TAMB'
          ACCEPT*,PAMB,TAMB
          TAMB=1.8*TAMB+32.
          RHOAMB=144.*PAMB/(53.34*(TAMB+460.))
          X=(1.4-1)/1.4
C OPEN A SPACE ON THE FLOPPY DISK TO STORE THE UNSTEADY DATA.
          WRITE(5,*)'ENTER THE RUN NUMBER(MUST BE TWO DIGITS)'
          ACCEPT 2,HPROB(7),HPROB(8)
2         FORMAT(2A1)
          OPEN(UNIT=8,NAME=HPROB,ACCESS='DIRECT',TYPE='NEW',
          1FORM='UNFORMATTED',RECORDSIZE=2048,INITIALSIZE=320)
1         WRITE(5,*)'HOME THE SCANIVALVE'
          WRITE(5,*)'STOP?;0=NO,1=YES'
          ACCEPT*,II
          IF(II.EQ.1)GO TO 99
          WRITE(5,*)'ENTER THE POINT NUMBER'
          ACCEPT*,IPOINT
C READ THE FREQUENCY COUNTER TO OBTAIN REV/SEC
          CALL IBRECV(SPEED1,17,'0')
          CALL IBIFC
C READ THE SCANIVALVE AND DETERMINE CHANNEL NUMBER
C SCANS EACH CHANNEL 30 TIMES AND TAKES THE AVERAGE
          DO 10 J=1,48
          CALL SCAN(KL,IPOS,ID)
          CALL CHAN(IPOS,ICHN)
          ICH=ICHN+1
          IF(ICH.GT.48)ICH=ICH-48
          P(ICH)=0.
          DO 20 K=6,30
20        P(ICH)=P(ICH)+FLOAT(ID(K))/25.
10        CONTINUE
C THE ZERO SHIFT IN THE TRANSDUCER DURING A RUN IS
C CORRECTED FOR BY HAVING TWO CHANNELS VENTED TO
C ATMOSPHERE(PREF) AND SUBTRACTING THESE TWO FROM THE
C OTHER CHANNELS.
          PREF=(P(47)+P(48))/2.
```

(CONTINUED)

```
C THE PRESSURE IS CONVERTED FROM A DIGITAL SIGNAL TO
C ENGINEERING UNITS.
      DO 11 N=1,48
11    P(N)=50.*(P(N)-PREF)/2048.
      DO 12 NN=1,48
12    P(NN)=P(NN)+PAMB
      PST=(P(31)+P(32))/2.
      PSS=(P(27)+P(28)+P(29)+P(30))/4.
C READ THE TEMPERATURE MULTIPLEXER
      CALL AD(0,6,T,IER)
      DO 40 LL=1,7
40    T(LL)=1.8*T(LL)+32.+460.
C READ COUNTER AGAIN
      CALL IBRECV(SPEED2,17,'0')
      CALL IBIFC
C TRANSFER SPEED TO ENGINEERING UNITS
      DECODE(10,3,SPEED1(6))RPS1
      DECODE(10,3,SPEED2(6))RPS2
3     FORMAT(E10.0)
      RPM=30.*(RPS1+RPS2)
      WRITE(5,*)'COMP PRESS=',PST,'TURB PRESS=',P(45)
      WRITE(5,*)'RPM=',RPM,'COMP TEMP=',T(2)
      WRITE(5,*)'DO YOU WANT THIS POINT?;0=NO,1=YES'
      ACCEPT*,L
      IF(L.EQ.0)GO TO 1
C ENTER THE NOZZLE TOTAL PRESSURE(PTN),THE TURBINE EXIT STATIC
C PRESSURE(PVAC),AND THE COMPRESSOR INLET STATIC PRESSURE.
      WRITE(5,*)'ENTER PTN,PVAC,AND MCOMP'
      ACCEPT*,PTN,PVAC,FMCOMP
      WRITE(6,*)'DATE:',IMONTH,'/',IDAY,'/',IYEAR
      WRITE(6,*)'ATM. PRESS.=',PAMB,'PSI'
      WRITE(6,*)'ATM. TEMP.=',TAMB,'F'
      WRITE(6,*)'POINT NO.=',IPOINT
      WRITE(6,*)'**THE INPUT DATA IS:**'
      WRITE(6,*)'PTN=',PTN,'PVAC=',PVAC,'MC=',FMCOMP
      PTN=PTN+PAMB
      PVAC=PAMB-PVAC*14.696/30.
C FIND COMPRESSOR MASS FLOW
      FMCOMP=RHOAMB*.1044*SQRT(334.6096*FMCOMP/RHOAMB)
      PRTT=PST/PAMB
      PRTS=PSS/PAMB
      PS3=(P(4)+P(10))/2.
      PS4=(P(6)+P(12))/2.
      PRITT=P(46)/PAMB
      DIFF=PS4-PS3
      CPDS=0.
```

(CONTINUED)

```
C FIND STATIC PRESSURE RISE OF VANELESS DIFFUSER
      IF(DIFF.NE.0.)CPDS=(P(46)-PS3)/DIFF
      ETACTT=((PRTT)**X-1.)/(T(2)/T(1)-1.)
      ETACTS=((PRTS)**X-1.)/(T(2)/T(1)-1.)
      ETICTT=((PRITT)**X-1.)/(T(2)/T(1)-1.)
      ERTS=P(45)/PVAC
      G=PAMB/14.696
      TH=(TAMB+460.)/545.
C CORRECT MASS FLOW AND SPEED TO 14.696 AND 545 DEG. R
      CORM=FMCOMP*SQRT(TH)*60./G
      CORN=RPM/SQRT(TH)
      WRITE(5,*)'ARE YOU IN STALL?:0=NO,1=YES'
      ACCEPT*,ISTALL
      IF(ISTALL.NE.0)GO TO 1000
1001  DO 30 M=1,48
30    WRITE(6,*)'PRESSURE',M,'=',P(M),'PSI'
      DO 50 MM=1,7
50    WRITE(6,*)'TEMPERATURE',MM,'=',T(MM),'DEG.R'
      WRITE(6,*)'PTN=',PTN,'PVAC=',PVAC
      WRITE(6,*)'RPM=',RPM,'MCOMP=',FMCOMP
      WRITE(6,*)'*********SPEED LINE DATA SS *********'
      IF(ISTALL.NE.0)WRITE(6,*)'THE COMPRESSOR IS IN STALL'
      WRITE(6,*)'PRESSURE RATIO T-T=',PRTT
      WRITE(6,*)'EFFICIENCY T-T=',ETACTT
      WRITE(6,*)'PRESSURE RATIO T-S=',PRTS
      WRITE(6,*)'EFFICIENCY T-S=',ETACTS
      WRITE(6,*)'CORRECTED MASS FLOW=',CORM,'LBM/MIN'
      WRITE(6,*)'CORRECTED SPEED=',CORN,'RPM'
      WRITE(6,*)'ROTOR PRESSURE RATIO T-T=',PRITT
      WRITE(6,*)'ROTOR EFFICIEMCY T-T=',ETICTT
      WRITE(6,*)'DIFFUSER STATIC PRESS RISE COEF.=',CPDS
      WRITE(6,*)'EXPANSION RATIO T-S=',ERTS
      WRITE(6,*)'****************************************'
      WRITE(6,*)'****************************************'
C PLOT OVERALL CHARACTERISTIC ON SCREEN
      CALL GRINIT(IBUF)
      CALL GRSCAL(IBUF,0.,1.,0.,2.5,0)
      XA(IPOINT)=CORM/60.
      YA(IPOINT)=PRTT
      CALL GRAPHS(IBUF,65,XA,YA,IPOINT,0.,0)
      PAUSE
      CALL VTCLR
      GO TO 1
C READ DYNAMIC RESPONSE PROBES AND STORE DATA ON FLOPPY DISK
1000  INCR=INCR+1
      J=2*INCR-1
      K=2*INCR
      CALL PROB(ID1,ID2)
      WRITE(8'J)(ID1(LL),LL=1,2048)
      WRITE(8'K)(ID2(MM),MM=1,2048)
      GO TO 1001
99    CLOSE(UNIT=8)
      END
```

Program to Read Scanivalve

```
          .GLOBL SCAN
SCAN:     MOV (R5)+,R0
          CLR @#171770
          MOV @(R5)+,@#171772
          CLR R1
          MOV #35,R2
ADDRES:   TST @#171770
          BPL ADDRES
          MOV @#171774,@(R5)+
          MOV (R5)+,R3
LOOP1:    MOV #4402,@#170400
          MOV #100,@#170402
LOOP2:    TST @#170400
          BPL LOOP2
          MOV @#170402,(R3)+
          INC R1
          CMP R2,R1
          BPL LOOP1
          RTS PC
          .END SCAN
```

Program to Determine Scanivalve Channel Number

```
C THIS PROGRAM CALCULATES S/V CHANNEL NO.  (ICHN)
C FROM S/V DATA (IPOS)
          SUBROUTINE CHAN(IPOS,ICHN)
          IF(IPOS.LT.10)GO TO 40
          IF(IPOS.GT.30)GO TO 10
          ICHN=IPOS-6
          GO TO 50
10        IF(IPOS.GT.42)GO TO 20
          ICHN=IPOS-12
          GO TO 50
20        IF(IPOS.GT.60)GO TO 30
          ICHN=IPOS-18
          GO TO 50
30        ICHN=IPOS-24
          GO TO 50
40        ICHN=IPOS
50        CONTINUE
          RETURN
          END
```

Program to Read Dynamic Response Pressure Transducers

```
        .GLOBL PROB
PROB:   MOV (R5)+,R0
        MOV (R5)+,R1
        MOV (R5)+,R2
        CLR R3
        MOV #1402,@#170400
LOOP1:  MOV #101,@#170402
LOOP2:  TST @#170400
        BPL LOOP2
        MOV @#170402,(R1)+
        MOV #102,@#170402
LOOP3:  TST @#170400
        BPL LOOP3
        MOV @#170402,(R2)+
        INC R3
        CMP #3777,R3
        BPL LOOP1
        RTS PC
        .END PROB
```

FAST FOURIER TRANSFORM PROGRAM

```
C THIS PROGRAM PERFORMS AN FFT ON THE HIGH RESPONSE DATA
C AND PLOTS THE RESULTS IN THE FREQUENCY DOMAIN.
C     ASSIGN DY1: 8
          BYTE HPROB(13)
          DIMENSION ID1(2048),ID2(2048),IMAG(2048),WR(2048)
          COMMON WR,ISCALE
          DATA HPROB/'D','Y','1',':','U','S',' ',' ',
     1'.','D','A','T',0/
          DATA IMAG/2048*0/,I/0/
          WRITE(5,*)'ENTER THE RUN NUMBER(MUST BE 2 DIGITS)'
          ACCEPT 2,HPROB(7),HPROB(8)
2         FORMAT(2A1)
          OPEN(UNIT=8,NAME=HPROB,ACCESS='DIRECT',TYPE='OLD',
     1FORM='UNFORMATTED',RECORDSIZE=2048,INITIALSIZE=320)
1         I=I+1
          J=2*I-1
          K=2*I
          READ(8'J)(ID1(L),L=1,2048)
          READ(8'K)(ID2(M),M=1,2048)
C SUBTRACT OUT THE ZERO READING
          DO 11 IR= 1,2048
          ID1(IR)=ID1(IR)-2048
11        ID2(IR)=ID2(IR)-2048
          IERROR=0
          ISCALE=0
C PERFORM A FFT ON CHANNEL 1
          CALL FFT(IERROR,2048,ID1,IMAG,0,ISCALE)
          WRITE(5,*)'CHANNEL 1 ERROR=',IERROR
          DO 10 IJ=1,2048
          WR(IJ)=SQRT(FLOAT(ID1(IJ))**2+FLOAT(IMAG(IJ))**2)
10        IMAG(IJ)=0
C PLOT THE FFT RESULTS FOR CHANNEL 1
          CALL PLTFFT
          IERROR=0
          ISCALE=0
C PERFORM A FFT ON CHANNEL 2
          CALL FFT(IERROR,2048,ID2,IMAG,0,ISCALE)
          WRITE(5,*)'CHANNEL 2 ERROR=',IERROR
          DO 20 IK=1,2048
          WR(IK)=SQRT(FLOAT(ID2(IK))**2+FLOAT(IMAG(IK))**2)
20        IMAG(IK)=0
C PLOT THE FFT RESULTS FOR CHANNEL 2
          CALL PLTFFT
          WRITE(5,*)'DO YOU WANT TO CONTINUE?(1=YES,0=NO)'
          ACCEPT*,ICONT
          IF(ICONT.NE.0)GO TO 1
          CLOSE(UNIT=8)
          END
```

PLOT PROGRAM FOR FAST FOURIER TRANSFORM RESULTS

```
C THIS PROGRAM PLOTS THE TRANSFORMED DATA ARRAY USING THE
C HIPLOT PLOTTER.
      SUBROUTINE PLTFFT
      DIMENSION WR(2048),IBUF(20)
      BYTE CHAR(45),FILNAM(10),SCR(50)
      COMMON WR,ISCALE
      DATA FILNAM/'A','S','C','I','I','.','C','H','R',0/
      TYPE*,'PLOTTING THE REAL ARRAY OF TRANSFORMED DATA'
      IC=1
C THE DIMENSIONS OF THE X AND Y AXIS
      XLLEFT=1.5
      YLLEFT=1.2
      XUPRT=9.
      YUPRT=7.
      TYPE*,'ENTER XMIN,XMAX'
      ACCEPT*,XMIN,XMAX
      TYPE*,'ENTER THE ABSCISSA INCREMENT'
      ACCEPT*,XINC
      WR(1)=0.
      YMAX=WR(2)
      YMIN=WR(2)
C FIND THE MAX. AND MIN. OF THE DATA ARRAY
      DO 10 I=3,2048
      IF(WR(I).GT.YMAX)YMAX=WR(I)
10    IF(WR(I).LT.YMIN)YMIN=WR(I)
      YMAX=YMAX*2**ISCALE
      YMIN=YMIN*2**ISCALE
C THE CHARACTER SIZE
      SIZE=.25
      CALL PLTSET(IBUF,1,10)
      CALL PLTSCL(IBUF,XMIN,XMAX,YMIN,YMAX,XLLEFT,YLLEFT,
     1XUPRT,YUPRT)
      CALL PLTAXS(IBUF,SCR,FILNAM,4)
      Y=WR(IC)*2**ISCALE
      CALL PLTSMV(IBUF,XMIN,Y)
      CALL PENDN
      XINC1=XINC
100   IC=IC+1
      Y=WR(IC)*2**ISCALE
      CALL PLTSMV(IBUF,(XMIN+XINC1),Y)
      XINC1=XINC1+XINC
      IF((XMIN+XINC1).GT.XMAX)GO TO 200
      GO TO 100
200   CALL PENUP
      CALL PLTSMV(IBUF,XMIN,YMIN)
      DO 888 KT=1,2
      IF(KT.EQ.1)TYPE*,'LABELLING TITLE:ENTER(X,Y) IN IN.'
      IF(KT.EQ.2)TYPE*,'LABELLING X-AXIS:ENTER(X,Y) IN IN.'
      ACCEPT*,XT,YT
```

(CONTINUED)

```
      TYPE*,'ENTER THE LABELLING STRING'
      ACCEPT 567,NCHAR,(CHAR(I),I=1,NCHAR)
567   FORMAT(Q,45A1)
      CALL PLTMOV(IBUF,XT,YT,1)
      CALL PLTSTR(IBUF,CHAR,NCHAR,SIZE,0,FILNAM)
      CALL PLTSMV(IBUF,XMIN,YMIN)
888   CONTINUE
      TYPE*,'LABELLING Y-AXIS: ENTER (X,Y) IN IN.'
      ACCEPT*,XT,YT
      TYPE*,'ENTER THE LABELLING STRING'
      ACCEPT 567,NCHAR,(CHAR(I),I=1,NCHAR)
      CALL PLTMOV(IBUF,XT,YT,1)
      CALL PLTSTR(IBUF,CHAR,NCHAR,SIZE,1,FILNAM)
      CALL PLTSMV(IBUF,XMIN,YMIN)
      CLOSE(UNIT=10)
      RETURN
      END
```

PRESSURE VERSUS TIME PROGRAM

```
C THIS PROGRAM CONVERTS THE HIGH RESPONSE DATA FROM A
C DIGITAL SIGNAL TO PRESSURE AND PLOTS THE RESULTS.
C CHANNEL 1 SENSITIVITY=2.40PSI/MV
C CHANNEL 2 SENSITIVITY=1.89PSI/MV
C     ASSIGN DY1: 8
          BYTE HPROB(13)
          DIMENSION ID1(2048),ID2(2048),WR(2048)
          COMMON WR
          DATA HPROB/'D','Y','1',':','U','S',' ',' ',
     1'.','D','A','T',0/
          WRITE(5,*)'ENTER THE RUN NUMBER(MUST BE 2 DIGITS)'
          ACCEPT 2,HPROB(7),HPROB(8)
2         FORMAT(2A1)
          OPEN(UNIT=8,NAME=HPROB,ACCESS='DIRECT',TYPE='OLD',
     1FORM='UNFORMATTED',RECORDSIZE=2048,INITIALSIZE=320)
1         WRITE(5,*)'ENTER THE POINT NUMBER'
          ACCEPT*,I
          J=2*I-1
          K=2*I
          READ(8'J)(ID1(L),L=1,2048)
          READ(8'K)(ID2(M),M=1,2048)
C CONVERTING THE PRESSURE TO ENGINEERING UNITS
          DO 11 IR= 1,2048
11        WR(IR)=(FLOAT(ID1(IR))-2048.)/2048.*(5.*2.48*5.)
C PLOT THE PRESSURE VERSUS TIME RESULTS FOR CHANNEL 1
          CALL PLTPR
          DO 12 IS=1,2048
12        WR(IS)=(FLOAT(ID2(IS))-2048.)/2048.*(5.*1.89*5.)
C PLOT THE PRESSURE VERSUS TIME RESULTS FOR CHANNEL 2
          CALL PLTPR
          WRITE(5,*)'DO YOU WANT TO CONTINUE?(1=YES,0=NO)'
          ACCEPT*,ICONT
          IF(ICONT.NE.0)GO TO 1
          CLOSE(UNIT=8)
          END
```